Systemic Multi-Omics Analysis Reveals Interferon Response Heterogeneity and Links Lipid Metabolism to Immune Alterations in Severe COVID-19

Ronaldo Lira-Junior[1†], Anoop T Ambikan[2†], Axel Cederholm[3,†], Sefanit Rezene[2†], Flora Mikaeloff[2], Sara Svensson Akusjärvi[2], Ahmet Yalcinkaya[3], Xi Chen[2], Maike Sperk[2], , Maribel Aranda-Guillén[4], Hampus Nordqvist[5], Carl Johan Treutiger[5,6], Nils Landegren[3,4], Ujjwal Neogi[2], and Soham Gupta[2*]

[1]Division of Oral diagnostics & Surgery, Department of Dental Medicine, Karolinska Institutet, Huddinge, Sweden
[2]The Systems Virology Laboratory, Division of Clinical Microbiology, Department of Laboratory Medicine, Karolinska Institute, 141 52 Stockholm, Sweden
[3] Science for Life Laboratory, Department of Medical Biochemistry and Microbiology, Uppsala university, Uppsala, Sweden
[4]Centre for Molecular Medicine, Department of Medicine (Solna), Karolinska Institute, Stockholm, Sweden
[5]Department of Infectious Diseases/Venhälsan, South General Hospital, Stockholm, Sweden
[6]Department of Medicine Huddinge, Division of Infectious Diseases, Karolinska Institute, I73, Karolinska University Hospital, Huddinge, 141 86 Stockholm, Sweden

[†]Authors contributed equally
*Corresponding Author

Correspondance to: soham.gupta@ki.se

Competing Interest: None to declare

Keywords: Interferon Stimulated Genes (ISGs), type-I interferons, COVID-19, Neutrophil activation, Interferon autoantibody, metabolic changes

Abstract:

The immune response to SARS-CoV-2 is highly heterogeneous, with interferon (IFN)-stimulated gene (ISG) expression playing a dual role in antiviral defense and immune dysregulation. To understand the broader implications of IFN-driven immune responses, we analyzed whole-blood transcriptomics, plasma proteomics, metabolomics, and immune cell profiling in COVID-19 patients and uninfected controls. Patients were stratified into low (LIS), moderate (MIS), and high (HIS) ISG expression clusters, independent of acute disease severity. HIS patients exhibited elevated inflammatory mediators (S100A8/A9, Neopterin) and altered metabolic profiles, yet immune activation patterns varied. Plasma from HIS cases induced differential activation in healthy neutrophils and monocytes, with severe HIS plasma showing reduced activation, suggesting the presence of suppressive soluble factors. Metabolomic analysis revealed widespread lipid metabolism dysregulation, including reductions in phospholipids, sphingolipids, and plasmalogens, which correlated with impaired immune activation. Branched-chain lipids and tryptophan metabolism products correlated strongly with monocyte and neutrophil activation, linking metabolic shifts to immune regulation. Despite IFN autoantibody detection in a subset of patients, no direct association with ISG expression was observed. These findings suggest that IFN-driven immune-metabolic dysregulation may persist beyond acute infection, contributing to post-viral inflammation, immune dysfunction, and susceptibility to long COVID or autoimmune-like sequelae. The interplay between IFN signaling, mitochondrial function, and lipid metabolism highlights novel therapeutic targets for immune modulation in viral infections and chronic inflammatory conditions. Understanding these immune signatures may inform precision medicine approaches in post-viral syndromes and immunometabolic disorders.

Introduction:

The coronavirus disease 2019 (COVID-19) is caused by the severe acute respiratory syndrome coronavirus 2 (SARS-CoV-2) which exhibits a wide range of clinical manifestations, from asymptomatic infection to severe respiratory distress with systemic complications [1]. A key feature of severe infection is hyperinflammation driven by dysregulated immune signaling caused by proinflammatory cytokines, including alterations in interferon (IFN) responses [2]. Interferons (IFN) are specialized type of cytokines that mediate antiviral defense upon viral RNA recognition by receptors such as RIG-I or MDA-5 receptors [3]. IFNs induce the interferon-stimulated genes (ISGs) through a signaling cascade, activating three major IFN-classes: type-I IFN (IFN-α, -β, -ε, -κ, -ω), type-II (IFN-γ), and type-III (IFN-λ) [4]. While these IFNs signal through distinct receptors, they share downstream ISG activation, with significant overlap between type-I and type-III IFN responses [5, 6].

Interferons (IFNs) are among the earliest antiviral responses, with an early and robust response being critical for effective viral clearance and protection against SARS-CoV-2 infection [7]. However, genetic defects and presence of specific IFN-blocking autoantibodies can dampen their antiviral role and cause an inability to control SARS-CoV-2 replication, leading to a more severe disease [8, 9]. While some studies report a suppressed IFN-response in severe cases [10], others describe an elevated ISG expression with heightened inflammation, which correlates with worse disease outcomes [11]. SARS-CoV-2 is known to actively disrupt innate immune responses, contributing to dysregulated IFN signaling [12]. In murine models of human coronavirus infection, a delayed type-I IFN response has been linked to excessive monocyte and macrophage activation, driving proinflammatory cytokine storms [4]. Beyond the immune response, metabolic alterations have emerged as critical determinants of COVID-19 severity. IFN signaling can influence lipid metabolism, glycolysis, and amino acid pathways [13]. These metabolic shifts can, in turn, modulate immune cell function and inflammatory outcomes [13]. Furthermore, the dysregulation in IFN response can induce both autoimmune and non-autoimmune inflammatory responses [14]. Autoantibodies against type-I IFNs have been implicated in modifying IFN signaling in a subset of patients, although their precise role in disease progression remains complex and context-dependent [9, 15]. Thus, the efficient viral clearance and disease outcome hangs in a balance between IFN response and inflammation. There is considerable multifariousness in the IFN-

response and understanding both the protective and aberrant responses can aid in the development of immunomodulatory therapeutic strategies.

Beyond acute infection, IFN response heterogeneity extends beyond COVID-19 severity, influencing post-viral immune dysregulation, persistent inflammation, and metabolic dysfunction. Emerging evidence suggests that dysregulated ISG expression may contribute to post-viral syndromes such as long COVID, where prolonged immune activation and metabolic shifts are implicated in sustained fatigue, neurological symptoms, and cardiovascular complications [16]. Additionally, IFN-driven metabolic reprogramming, particularly disruptions in lipid and amino acid metabolism, may underlie broader immune dysfunctions, including autoimmune-like sequelae [17]. Understanding the interplay between IFN signaling, immune metabolism, and inflammatory resolution is therefore critical not only for COVID-19 but also for broader applications in chronic inflammatory and post-viral syndromes.

In this study, we investigate biological perturbations associated with ISG expression patterns in COVID-19 patients, stratifying individuals based on ISG-driven clustering (low-ISG score: LIS, moderate-ISG score: MIS, and high-ISG score: HIS). Using multi-omics data (plasma proteomics and metabolomics), autoantibody screening, and immune activation analyses, we explore how IFN response heterogeneity is linked to immune and metabolic alterations. Our findings reveal a stochastic relationship between ISG expression and immune cell activation, along with significant perturbations in lipid and amino acid metabolism. These insights offer a framework for understanding the complex interplay between IFN signaling, immune responses, and metabolic adaptation in COVID-19, which could aid in personalized treatment strategies.

Results:

IFN-signatures in COVID-19 disease severity:

IFNs can induce several ISGs that have an antiviral function. In our previous *in vitro* studies, we have observed cell type-specific ISG-signatures upon SARS-CoV-2 infection and the ability of SARS-CoV-2 to dysregulate the IFN-response [18]. In the COVID-19 disease, the imbalanced IFN response has been linked to the severity. To investigate the link between IFN-signaling and

disease severity in hospitalized patients, we used RNA-seq data from 21 COVID-negative control (HC) , 10 Convalescent (conv), 28 SARS-CoV-2 infected Mild-disease (mild) and 11 SARS-CoV-2 infected Severe-disease (severe) patients (Figure 1A) previously described by us [19]. In the transcriptomics data, we analyzed genes linked to interferon responses in the type-I IFN (IFN-α/β) signaling pathway (R-HSA-909733), type-II IFN (IFN-γ) signaling pathway (R-HSA-877300), and antiviral ISG pathway (R-HSA-1169410) (Table S1), with several ISGs overlapping across these pathways. Both the mild and severe patient groups showed a significant increase in expression of ISGs that mainly belonged to type-I IFN signaling (FDR<0.05, Figure 1B). To determine patient-specific effects on the enhanced IFN response observed in the mild and severe COVID-19, we computed three ISG scores for type-I, -II, and antiviral signaling pathways in each sample by summing the Z-scores of all genes within the ISG set in a given pathway [20] (Table S2). A significant increase in ISG score for all three pathways was observed in mild disease compared to healthy, while no difference was seen between the mild and severe groups (Figure 1C, Mann Whitney U test, *p*-value<0.05). Additionally, visualization of ISG expression among the samples revealed distinct gene expression patterns between patients in mild and severe categories, warranting further investigation (Figure 1B).

IFNs activate ISGs via the JAK-STAT pathway. At the transcript level, most IFN gene expressions were very low (TPM <1) or undetectable, except for IFN-λ1 and IFN-γ, which significantly decreased in severe cases (Figure S1). We also measured IFN-I, -II, and -III levels (IFN-α2, IFN-β, IFN-λ1, IFN-λ2/3, IFN-γ) in patients' plasma using a FACS-based LEGENDplex assay to assess their role in ISG activation. Due to low concentrations, median fluorescence intensity (MFI) was used for analysis. No significant changes were observed in IFN levels in COVID-19 patients (Kruskal-Wallis test, FDR > 0.05, Figure 1D, Table S3).

COVID-19 patient stratification based on the ISG expression:

The heterogeneity of IFN-levels and ISG expression score between mild and severe groups was characterized by uniform distribution in the mild group but a bimodal distribution in the severe group (five patients showing ISG scores above one and six near zero as shown in Figure 1C), prompted re-categorization of all samples based on their transcriptomic ISG profiles. To this end, we performed a robust hierarchical consensus clustering of the patients based on the ISGs from

our transcriptomics data. This clustering grouped the subjects into three categories based on a consensus matrix and visualized through PCA analysis (Figures 2A, Figure S2). Clusters were henceforth named according to the ISG scores for the three IFN pathways: low-ISG score (LIS), resembling the healthy control (HC) pattern; moderate-ISG score (MIS); and high-ISG score (HIS) (Mann Whitney U test, p-value<0.05, Figure 2B-2C). The alignment of these clusters with previous clinical categorizations is displayed in Figure 2B.

Presence of IFN-I autoantibodies in patients with low ISG expression:

Inborn errors of IFN-immunity and neutralizing autoantibodies against IFNs have been associated with the dysregulated immune response and COVID-19 severity [8, 9]. Building on this, we explored any impact of IFN autoantibodies within these ISG-specific clusters. An in-house autoantibody-array with broad coverage of type I, type II, and type III IFNs identified samples with a fluorescent intensity above the cut-off of mean+7 standard deviations (SD) of healthy controls (HC) as positively reactive for the antigens and are marked by star symbols in the heatmap presented in Figure 2D. Autoantibodies to subtypes of IFNA (n= 5), IFNW1 (n= 1), IFNB (n=1), and IFNL1/IL29 (n= 1) were reactive in COVID19 patients (n=5), of which 3/11 and 2/28 were detected in the severe and mild groups respectively. Interestingly, autoantibody reactivities against IFNA subtypes (n=3) and IFN L4 (n=1) were also noted in the convalescent group (27%; n=3). Among the COVID-19 patients, most of the patients (3/6) with presence of any reactive IFN autoantibodies belonged to MIS, while only one patient each from LIS (all tested anti-IFNA subtypes, -IFNB1, -IFNW1 and -IFNL4) and HIS (only anti-IFNA2) showed IFN-autoantibody reactivities. Three of the obese patients showed presence of reactive antibodies against at least 4 of the IFNA subtypes. Additionally, antibody reactivities against GM-CSF (LIS:1 and MIS:1) and IL-12 (HIS:1) were also detected (Figure 2D).

To assess the functional impact of the screened autoantibodies on interferon activity and the observed immune dysregulation, Type-I IFN neutralization assays were conducted on samples identified reactive above threshhold for IFN autoantibody and other cytokines. Using a dual-luciferase ISRE reporter assay system, stimulated with IFNA2, neutralizing capacity of the patient plasma was determined. A heatmap of percentage inhibition is shown in Figure 2D; bottom row. Among the six patients with reactive IFN autoantibodies identified in the screening assay, four

exhibited >80% neutralization of IFNα2, with one each from LIS (1/1) and HIS (1/1), and two from MIS (2/3). Additionally, one MIS sample that showed reactivity against GM-CSF also demonstrated IFNα2 neutralization capacity. Notably, only the patient in the HIS group presented with severe disease. Furthermore, one of the three convalescent plasma samples displayed type-I IFN-neutralizing activity. Overall, we did not observe any clear association between IFN autoantibodies and the clinical severity of COVID-19 or the ISG expression.

In our array we also examined the antibody reactivities to the SARS-CoV-2 nucleocapsid protein, spike protein and RBD domain. Remarkably, HIS showed reduced reactivities for the spike and the RBD antibodies, unlike LIS and MIS which resembled convalescent reactivites (Figure 2E). A potentially more robust antibody response against Nucleocapsid protein irrespective of ISG expression status suggests its potential to be an effective immunogen and has implications for both vaccines and diagnostics.

Plasma Proteomics Reveals a Progressive Increase in Inflammation with Higher ISG Expression:

To investigate the relationship between ISG expression and systemic inflammation, we analyzed the plasma inflammatory cytokines measured using Olink onco-immunology panel [21] across ISG-defined clusters. Principal Component Analysis (PCA) of plasma proteomics data showed a clear segregation of patient clusters, mirroring the ISG score-based classification (Figure 3A). Samples from healthy controls (HC) and convalescents were closely grouped, suggesting a similarity in their plasma proteomic profile. Conversely, LIS samples clustered nearest to HC and convalescents, whereas MIS and HIS samples progressively diverged, reflecting an increasing inflammatory burden with higher ISG expression. HIS exhibited the greatest deviation from rest of the clusters along PC1 (47.04% variation), reinforcing the hypothesis that heightened ISG responses are associated with distinct inflammatory signatures. To further delineate specific inflammatory mediators linked to ISG expression, we performed hierarchical clustering using the Olink plasma proteomic data (Figure 3B). The heatmap displaying the hierarchical clustering employing complete linkage and Euclidean distance revealed distinct inflammatory signatures across ISG clusters, with a progressive increase in inflammatory cytokines from LIS to HIS (Figure 3B). Notably, several key inflammatory cytokines, including CXCL10, CXCL11, MCP-2, MCP-

3, IFN-γ, IL-10, and TNF showed a gradual transition and were significantly elevated in HIS compared to LIS (LIMMA, FDR < 0.05, Table S4), suggesting a chemokine-driven inflammatory process linked to interferon signaling. Additionally, IL-6 and TNF, both central mediators of cytokine storm, were particularly upregulated in HIS, highlighting a potential role in driving disease severity.

Enhanced type-I and type-II ISG expression in COVID-19 patients reshapes lipid and amino acid metabolism:

Increasing evidence suggests a crosstalk between cellular metabolism and IFN-signaling during viral infection. Type-I IFN has been shown to promote glycolysis [13], modulate lipid synthesis in macrophages [22, 23], as well as increase fatty acid oxidation and oxidative phosphorylation (OXPHOS) in infected plasmacytoid dendritic cells (pDCs) [24]. ISGs induced by IFNs also regulate the cellular central carbon metabolism [25]. In order to investigate how IFN signaling and metabolic pathways are linked during COVID-19 infection, we analyzed the ISGs cluster specific changes in the global plasma metabolomics data [21], providing insight into global metabolic shifts, particularly in lipid and amino acid metabolism, which are central to immune function and energy homeostasis. Principal Component Analysis (PCA) of metabolomics data demonstrated a clustering pattern that closely resembled ISG-defined groups (Figure 3C). LIS samples were positioned closer to HC and convalescent samples, indicating minimal metabolic alterations. In contrast, MIS and HIS samples showed a progressive divergence from HC, with HIS exhibiting the greatest metabolic shift, suggesting a significant metabolic dysregulation in patients with high ISG scores. An UpSet plot analysis (Figure 3D) was further generated to visualize and identify the most differentially altered metabolites across ISG-defined clusters. The highest number of metabolic alterations was observed in the HIS vs. LIS (LIMMA, FDR < 0.05, Table S5) comparison, followed by HIS vs. MIS and MIS vs. LIS, indicating a progressive metabolic shift with increasing ISG expression. Among the significantly dysregulated metabolites, lipid metabolism exhibited the most profound changes, followed by disruptions in amino acid metabolism. The specific metabolic pathways altered across ISG-defined clusters is presented in the heatmap (Figure 3E) and revealed widespread metabolic dysregulation in HIS, particularly in lipid-related metabolites. Key lipid species, including several phospholipids, sphingolipids, and carnitines, were significantly reduced in HIS compared to LIS and MIS, indicating a potential

impairment in lipid metabolism. Amino acid metabolism was also affected, with downregulation of key amino acids such as arginine, gamma-carboxyglutamate, and 6-bromotryptophan in HIS. Both type-I and type-II ISG scores showed predominantly a negative association with the metabolites belonging to amino acid and lipid metabolism (Spearman correlation, p-value<0.05, Fig S4, Table S6), suggesting that the hyperinflammatory state during COVID-19 can cause disorder in lipid and amino acid metabolism. This metabolic shift may impact immune cell function, given that arginine depletion is associated with T-cell dysfunction and tryptophan metabolism is crucial for immunoregulation.

ISG Expression is Associated with Myeloid Cell Expansion and Enhanced Inflammatory Activation:

To investigate the relationship between ISG expression, immune cell composition, and systemic inflammation, we performed digital cell quantification (DCQ) using a reference signature of 18 blood cell types from the Human Protein Atlas [26] and the EPIC deconvolution algorithm [27]. The analysis revealed a progressive shift toward an innate pro-inflammatory state with increasing ISG expression. LIS patients exhibited an immune profile similar to healthy controls (HC), whereas MIS and HIS displayed a marked expansion of innate immune cells, particularly neutrophils and classical monocytes (Figure 4A, Figure S3, Table S7). Further phenotyping of phagocytic cells in a subset of samples confirmed a higher proportion of immature neutrophils in HIS and increased classical monocytes in both HIS and MIS (not statistically significant), reinforcing the association between ISG expression and inflammatory myeloid cell expansion (Figure S4).

To determine whether these expanded innate immune populations were also functionally activated, we measured plasma levels of S100A8/A9 and Neopterin, markers of neutrophil and monocyte activation. S100A8/A9, a neutrophil-derived alarmin involved in inflammatory signaling, was significantly elevated in HIS and MIS compared to LIS (Figure 4B; Kruskal-Wallis test, p-value < 0.05, Table S8), consistent with heightened neutrophil activation. Similarly, Neopterin, a marker of activated monocytes and macrophages, followed the same trend (Figure 4C), further supporting the association between higher ISG expression and myeloid cell-driven inflammation. Neutrophils, key effectors of innate immunity, are equipped with pathogen recognition receptors such as RIG-I and MDA5, which can induce IFN responses upon activation [28]. As part of this response,

neutrophils release S100A8/A9 (alarmin), a damage-associated molecular pattern (DAMP) that attracts immune cells and amplifies inflammatory signaling [29]. S100A8/A9 has been implicated in SARS-CoV-2 inflammatory pathogenesis [30], and its elevation in HIS and MIS further reinforces its role in ISG-driven inflammation.

Neutrophil activation can also lead to the formation of neutrophil extracellular traps (NETs), which interact with cytosolic DNA sensors such as cGAS and activate IFN pathways via cGAS-STING signaling [31]. To assess NET formation, we measured MPO:DNA complexes, a key indicator of NETosis. Interestingly, while MPO:DNA complexes were significantly increased in MIS, HIS did not show a corresponding rise (Figure 4D), suggesting that S100A8/A9-mediated inflammation, rather than NETosis, plays a dominant role in the ISG-high immune phenotype. Disease severity stratification revealed that S100A8/A9 and Neopterin were elevated in both mild and severe cases, whereas MPO:DNA levels did not significantly differ across disease severity categories (Figure S5), indicating that high ISG expression and inflammation are not exclusive to severe disease.

To further assess the relationship between ISG expression and immune cell shifts, we examined correlations between immune cell proportions and ISG scores. LIS showed a significant positive correlation with classical monocytes across all three ISG categories, while MIS correlated with additional immune subsets, including those indicated in Figure 4E (Spearman correlation, FDR < 0.05, Table S9). Notably, no immune cell type exhibited a significant positive correlation with ISG scores in HIS, suggesting that high ISG expression is associated with a more complex immune landscape rather than the expansion of specific immune cell types. These findings highlight that high ISG expression is strongly associated with innate immune activation, increased neutrophils and monocytes, and elevated inflammatory markers, yet the lack of correlation between ISG levels and specific immune subsets in HIS suggests a distinct, dysregulated immune state. Unlike MIS, NETosis does not appear to be a key driver, pointing to alternative IFN-driven inflammatory pathways. Given that HIS includes both mild and severe cases, further investigation is essential to determine the factors driving disease severity within this ISG-high group.

Metabolic and Immune Dysregulation Define Disease Severity in the High ISG-expressing Group by altering Neutrophil and Monocyte Activation:

Despite high ISG expression across all HIS patients, disease severity varies within this group, suggesting that immune activation alone does not fully explain progression to severe disease. Digital cell quantification (DCQ) analysis previously showed that HIS patients had significantly higher proportions of neutrophils and monocytes compared to other ISG clusters, alongside elevated levels of S100A8/A9 and Neopterin, markers of neutrophil and monocyte activation. These findings indicate that while innate immune activation is a defining feature of HIS, disease severity is not simply driven by further increases in myeloid cell expansion. Notably, no immune cell type exhibited a significant positive correlation with ISG scores within HIS, suggesting that functional alterations in immune activation or systemic factors such as metabolic and inflammatory mediators may be key determinants of severity. Additionally, unlike MIS, NETosis (as measured by MPO:DNA complexes) was not significantly elevated in HIS, further pointing to alternative IFN-driven inflammatory pathways contributing to disease severity. To determine these factors, we first assessed neutrophil and monocyte activation in response to patient plasma, followed by differential regulation analysis of inflammatory mediators (Olink) and metabolic alterations (metabolomics) to identify pathways influencing immune dysregulation.

To assess immune activation, we incubated healthy isolated neutrophils and PBMCs (for monocytes) with plasma from mild and severe cases and measured activation markers using flow cytometry. For neutrophils we used CD66b, CD11b, and CD62L, commonly used as activation markers to assess the phenotype of neutrophils, where CD66b and CD11b upregulation indicate activation and degranulation, while CD62L shedding reflects neutrophil activation and migration [32]. For monocytes we used CD169 (Siglec-1), a key marker for monocyte activation, particularly in response to type I interferons, and is involved in antigen capture and viral recognition [33]. Interestingly, plasma from severe cases induced lower neutrophil (Low CD66b and CD11b, and high CD62L) and monocyte (low CD169; $p<0.05$) activation compared to mild cases (Figure 5A), suggesting that the inflammatory environment in severe disease may suppress immune cell responsiveness rather than enhance activation. This raises the possibility that immune cells in severe cases are either refractory to further activation due to prior overstimulation or are influenced by suppressive factors in circulation.

To identify soluble mediators of disease severity in HIS, we analyzed inflammatory factors (Olink Immuno-oncology panel), comparing severe and mild cases using LIMMA (Table S10). MCP-3 (CCL7), HGF, and IL-6 were significantly elevated in severe HIS cases (Figure 5B, FDR < 0.05), suggesting their strong association with severity. MCP-3 (CCL7), a key monocyte-recruiting chemokine [34], aligns with the increased monocyte proportions observed in HIS, implicating monocyte-driven inflammation in severe disease. HGF, a regulator of tissue repair and immune modulation [35], may act as a compensatory response to inflammation-induced tissue damage, but its dysregulation in severe cases suggests immune dysfunction. IL-6, a major pro-inflammatory cytokine [36], is a hallmark of hyperinflammatory states and further supports an exaggerated immune response in severe HIS. These findings indicate that severity in HIS is not solely driven by ISG expression but rather by dysregulated inflammatory pathways involving monocyte recruitment (MCP-3), immune modulation (HGF), and systemic inflammation (IL-6). To further investigate the mechanisms of immune dysfunction, we next examined metabolic alterations and their link to immune activation markers.

Metabolomic profiling identified 36 significantly altered metabolites (Figure 5C, LIMMA FDR < 0.05, Table S11), with energy metabolism and lipid metabolism emerging as the most dysregulated pathways. TCA cycle intermediates, particularly citrate and aconitate, were significantly reduced in severe cases, suggesting mitochondrial dysfunction and impaired energy metabolism. The suppression of the TCA cycle in severe HIS cases may impair immune cell function, as mitochondrial energy production is essential for proper immune activation [37]. Lipid metabolism was also significantly disrupted, with reductions in plasmalogens, phosphatidylcholines, and sphingolipids in severe cases. Plasmalogens and phosphatidylcholines are essential for membrane stability and lipid raft formation, which regulate immune receptor clustering and signaling [38]. Their depletion in severe cases may impair immune cell communication and inflammatory resolution, contributing to dysregulated immune responses. Sphingolipids play a key role in apoptosis and immune cell survival, and their reduction in severe cases may contribute to immune cell dysfunction [39].

To establish direct links between metabolic changes and immune activation, we examined correlations between significantly altered metabolites and neutrophil/monocyte activation markers (FACS MFI) (Figure 5D; Table S12, Spearman correlation, p-value<0.05). Among the 36

significantly altered metabolites, 16 showed significant correlations with at least one immune activation marker, highlighting key metabolic-immune interactions. Notably, 6-bromotryptophan and branched-chain 14:0 dicarboxylic acid exhibited positive correlations with all tested activation markers, CD169 (monocyte activation), CD11b (neutrophil adhesion/migration), and CD66b (neutrophil degranulation and activation). This suggests that these metabolites may play a central role in immune activation across both monocyte and neutrophil populations. In addition, 1,2-dilinoleoyl-GPC (18:2II18:2) correlated with both CD169 and CD11b, further reinforcing the connection between lipid metabolism and innate immune activation. Interestingly, indoline-2-one**,** a xenobiotic metabolite derived from oxidized tryptophan metabolism, also showed significant correlation with CD169 and CD11b. The remaining metabolites primarily correlated with CD169, indicating a stronger association between metabolic changes and monocyte activation compared to neutrophil activation. This supports the hypothesis that monocyte-driven inflammation may be a key determinant of severity in HIS cases, potentially driven by metabolic shifts that influence monocyte activation and function. These findings suggest that severity in HIS is not only influenced by inflammatory mediators such as MCP-3 and HGF but also by distinct metabolic alterations, particularly in tryptophan metabolism, branched-chain lipid oxidation, and phospholipid remodeling. The correlation between the significant inflammatory mediators MCP-3, HGF and IL6 with the metabolites shows a negative trend (Figure S6). The strong negative correlation between lipid and amino acid metabolites with immune activation markers highlights a metabolic-inflammatory axis contributing to immune dysregulation, suggesting that targeting these metabolic pathways may provide new therapeutic opportunities to modulate excessive immune activation in severe HIS cases.

In a subset of patients, where PBMCs were available, we conducted western blot analysis to assess the protein expression levels of specific ISGs (Figure S7A). We then correlated these protein levels with the corresponding transcript levels obtained from the RNA sequencing data. Notably, we observed an intriguing observation: in mildly infected patients, there was a robust positive correlation (Spearmans' Rho > 0.6) between protein and transcript levels for ISG15, RIG-I, IRF3, and STING (Figure S7B and S7C). However, this correlation was no longer evident in patients with severe infection (Figure S7B and S7D). Despite a very small sample size, it is worth

mentioning that this finding raises the possibility of translational dysregulation, which may contribute to suboptimal antiviral ISG protein expression and ultimately result in disease severity.

Discussions:

The interferon (IFN)-signaling is a response that is activated immediately following virus infection plays a pivotal role in antiviral immunity, yet its dysregulation has been implicated in the pathogenesis of severe COVID-19. A balanced IFN response is crucial to eliminating viral infections while preventing excessive inflammation and immune-mediated damage. In the case of COVID-19 there has been much interest in studying this response due to its dual role in COVID-19 pathology [40-42]. On the one hand, a robust IFN response in early infection shows a protective role and milder disease outcome [4, 43]. The protective role is further strengthened by the fact that IFN-deficiency can lead to severe COVID-19 [8, 9]. On the other hand, hyperinflammation due to interferonopathy has been observed in severe and critical COVID-19 disease [44-46]. There are several mechanisms by which IFN induces hyperinflammation. TNF induces tolerance to TLR activation and can be blocked by IFNs or by IFN transcriptional and epigenetic control mechanisms [47, 48]. To further add to it, SARS-CoV-2 has developed IFN inhibitory mechanisms by which it can delay and dysregulate the IFN response [49, 50]. Thus, it is of interest to understand for which subject, or when the IFN-response will become harmful and cause disease severity. Beyond COVID-19, dysregulated IFN signaling has been implicated in a range of inflammatory and autoimmune disorders, including lupus, rheumatoid arthritis, and chronic viral infections. Persistent ISG expression and metabolic perturbations may contribute to long-term immune dysfunction, suggesting that mechanisms observed in COVID-19 could have broader implications for understanding chronic immune activation and post-viral syndromes.

Our findings highlight a heterogeneous ISG response among COVID-19 patients, independent of disease severity. The stratification of patients based on ISG expression revealed three distinct clusters—low ISG score (LIS), moderate ISG score (MIS), and high ISG score (HIS)—each characterized by differential immune activation, inflammatory marker expression, and metabolic reprogramming. This classification provides novel insights into the interplay between IFN signaling, innate immune activation, and metabolic dysregulation in COVID-19.

Neutralizing autoantibodies against IFNs can modulate ISG expression by binding to soluble IFNs and preventing their interaction with IFNAR receptors, thereby dampening JAK-STAT signaling and ISG activation [51]. In viral infections, reduced ISG expression can lead to increased viral replication and subsequent hyperinflammation [40]. Prior studies have reported that approximately 10% of life-threatening COVID-19 cases exhibit autoantibodies against IFN-α subtypes and IFN-ω, with these autoantibodies being largely absent in asymptomatic or healthy individuals [9]. Additionally, another study found autoantibodies against IFN-α subtypes and IFN-ω in 20% of critically ill COVID-19 patients, with a higher prevalence in older individuals [52]. In our cohort, IFN autoantibody screening detected reactive IFN-autoantibodies of any type in 27% of severe cases (3/11) and 7.1% of mild cases (2/28), predominantly in the MIS group. Additionally we have also detected reactivities against antibodies to GM-CSF (LIS:1 and MIS: 1) and IL12 (HIS:1). The high rate of presence of IFN autoantibodies as compared to other cohorts could be due to methodological differences though we have considered a stringent cut off of +7SD to the mean values of healthy, a higher cut off compared to other studies [53, 54]. Functional neutralization assays revealed that four out of six IFN autoantibody-reactive patients demonstrated >80% neutralization of IFN-α2, spanning LIS (1/1), MIS (2/3;), and HIS (1/1), with only the HIS patient being severe. Importantly, one convalescent plasma sample displayed type-I IFN-neutralizing activity, raising questions about the persistence of immune dysregulation post-infection and its implications for long-term immunity. Interestingly,to note that the MIS patient showing reactivity to GM-CSF also showed >80% neutralization of IFN-α2. Despite these findings, no clear association was observed between IFN autoantibody reactivities, disease severity, or ISG expression. Additionally, plasma levels of type-I and type-III IFN did not significantly differ between patient groups, and showed no correlation with whole-blood transcriptomic data. Unlike influenza, where IFN responses are readily detectable early in infection, most COVID-19 patients exhibited undetectable levels of type-I and -III IFNs [55], regardless of autoantibody status [10]. This reinforces the notion that high ISG expression in COVID-19 is predominantly driven by endogenous IFN signaling rather than external IFN supplementation. The presence of IFN autoantibodies in convalescent patients and the lower SARS-CoV-2 Spike and RBD antibody reactivities in HIS compared to LIS and MIS suggest potential long-term immune alterations.

Innate immune activation was a defining feature of HIS, as evidenced by increased neutrophil and monocyte proportions using DCQ and elevated plasma levels of S100A8/A9 and Neopterin, markers of neutrophil and macrophage activation, respectively. S100A8/A9, an alarmin associated with SARS-CoV-2 pathogenesis [56], was significantly elevated in HIS and MIS, reinforcing the link between ISG expression and innate immune activation. It has been established that SARS-CoV-2 infection triggers secretion of alarmin that in turn can activate aberrant immature neutrophils and lead to dysregulated immune response [30]. Neopterin, a marker of macrophage activation released upon IFN-γ induction [57], followed a similar pattern to S100A8/A9, further supporting the role of IFN-driven myeloid cell activation in HIS.

ISGs can be activated through both IFN-dependent JAK-STAT signaling and IFN-independent IRF3 activation [58, 59]. In COVID-19 pathogenesis, neutrophil activation can lead to the formation of NETs [60] that can induce a cGAS-dependent induction of IFNs through the cGAS-STING pathway [31]. Despite previous reports linking NETs to severe COVID-19 [61], our findings did not indicate any association of NETs with either disease severity or with HIS. Instead, NET formation was significantly increased in MIS, highlighting distinct immune activation patterns between ISG-defined clusters. These findings suggest that HIS severity is not primarily driven by NET-associated inflammation but rather alternative pathways of immune dysregulation.

Among the three ISG-defined groups, the HIS cluster exhibited distinct immune and metabolic profiles that necessitate further investigation. HIS patients showed a significantly heightened inflammatory response, with increased neutrophil and monocyte activation, yet not all HIS cases were severe. Interestingly, plasma from severe HIS cases induced lower neutrophil (low CD66b and CD11b, and high CD62L) and monocyte (low CD169; $p<0.05$) activation compared to mild cases. This suggests that the inflammatory environment in severe disease may suppress immune cell responsiveness rather than enhance activation.

To identify soluble mediators of severity in the HIS group, we analyzed plasma inflammatory markers. MCP-3 (CCL7), hepatocyte growth factor (HGF), and IL-6 were significantly elevated in severe HIS cases, implicating monocyte recruitment and immune dysregulation. MCP-3 is a potent monocyte chemoattractant [34], aligning with the observed monocyte expansion in HIS. HGF, which regulates tissue repair and fibrosis, has been linked to severe COVID-19 outcomes

[35]. IL-6, a well-established severity marker , further reinforces the hyperinflammatory state in severe HIS cases [36]. These findings suggest that HIS severity is driven by inflammatory mediators rather than excessive ISG expression alone. Additionally, metabolic constraints may actively suppress immune activation rather than simply being a consequence of inflammation. The depletion of key lipid metabolites and TCA cycle intermediates observed in severe HIS cases suggests a shift towards an energy-limited immune phenotype, where immune cells fail to mount an effective response due to inadequate metabolic support.

During viral infection, metabolic reprogramming of the immune cell occurs to meet the energy demands for innate immune signaling and there is an interdependency between them, and the viruses can hijack it for its own replication [62]. Metabolomic profiling revealed significant alterations in amino acid and lipid metabolism, with TCA cycle suppression being a prominent feature in severe HIS cases. Reduced levels of citrate and aconitate suggest mitochondrial dysfunction, impairing energy metabolism and immune cell function [37]. Lipid metabolism was also significantly disrupted, with reductions in plasmalogens, phosphatidylcholines, and sphingolipids. These lipids are essential for membrane stability and immune signaling [38, 39]. Their depletion in severe cases suggests impaired immune cell communication and inflammatory resolution, contributing to immune dysfunction. Recent studies analyzing COVID-19 cohorts from different geographical regions have identified similar metabolic and immune dysregulation patterns. For instance, a European study found perturbation of amino acid and lipid metabolisms in European COVID-19 patients [63]. While another study has observed higher levels of triglycerides, diglycerides, and fatty acids in fatal cases of Chinese population [64]. However, none of these studies have investigated their effect on the interferon responses. Viruses usurp cellular lipid pathways to use as their building blocks and energy for its propagation [65]. Virus infected cells shows a reduction in lipid biosynthesis that in turn induces IFN-I in a STING dependent manner [22]. This falls in line with our observation of lowered lipid metabolite levels in patients with high ISG expression. Lower lipid levels were further associated with the disease severity in HIS and MIS clusters, and the dysregulated lipids showed unique patterns in both the clusters, without any observable overlap. Lower levels of citrate and cis/trans-aconitase, metabolites belonging to central carbon metabolism were a unique feature of the severe COVID-19 patients belonging to HIS cluster. While citrate connects, TCA cycle to fatty acid metabolism, both citrate

and cis-aconitase support the production of itaconate that has anti-inflammatory and IFN-regulatory function and as well its derivatives have inhibitory effects on virus replication, including SARS-CoV-2 [66-68]. Additionally, the observed lowered lipid levels and TCA cycle intermediates were in plasma, and we do not know if they were due to increased accumulation within the cell to aid the virus replication. Correlation analyses with the markers of neutrophil (CD11b and CD66b) and monocyte (CD169) activation in the HIS group revealed that specific metabolic alterations, particularly in lipid and amino acid metabolism, were linked to these immune activation patterns. Cumulatively, these findings suggest that immune cells in severe cases may be refractory to further activation due to prior overstimulation or are influenced by suppressive factors in circulation. Understanding how metabolic constraints modulate immune cell function is crucial for developing targeted interventions.

Our study has several limitations. First, while we identified metabolic alterations in plasma, we did not measure intracellular metabolic changes in immune cells. Single-cell metabolomics could provide deeper insights into how immune cell metabolism is altered in different ISG clusters. Second, while we observed significant associations between metabolic markers and immune activation, causal relationships remain unclear. Future studies should use functional assays to determine whether metabolic interventions can modulate immune responses. Lastly, our cohort size was limited, and larger multi-center longitudinal studies are needed to validate these findings.

The findings of this study are multilayered and underscores the complexity of IFN responses in COVID-19 and highlights the interplay between inflammation, immune activation, and metabolic reprogramming. High ISG expression alone does not determine disease severity; rather, the combination of inflammatory mediators and metabolic constraints dictates disease progression. These findings suggest that targeting metabolic pathways such as replenishing TCA cycle intermediates or modulating lipid metabolism may improve immune responsiveness and mitigate disease severity in high ISG-expressing patients. Further research should explore therapeutic strategies aimed at restoring metabolic homeostasis to modulate immune responses effectively. A multi-omics approach integrating transcriptomics, proteomics, and metabolomics could refine COVID-19 treatment strategies and advance precision medicine approaches for future pandemics. Furthermore, understanding the link between IFN-driven immune modulation and metabolic reprogramming may pave the way for novel immuno-metabolic therapies. Strategies targeting

metabolic rebalancing, including lipid supplementation and restoration of TCA cycle intermediates, might enhance immune responses in viral infections, autoimmune diseases, and chronic inflammatory conditions beyond COVID-19.

Methods:

Study design and patients:

The study included both PBMCs and plasma from SARS-CoV-2 infected individuals (*n=39*) hospitalized in Stockholm, Sweden during May 2020. These individuals were separated into the category of mild (*n=28*) or severe (*n=11*) disease based on O_2 requirement (O_2 consumption <4 l/min and >4 l/min for mild and severe respectively). The cohort was further complemented with non-infected individuals (*n=31*), that was divided into convalescent form SARS-CoV-2 infection (*n=10*) and non-infected (*n=21*). The clinical and demographic parameters of the cohort are as earlier described [19, 21]. The study was approved by the Swedish Ethical Review Authority (dnr 2020-01865). All individuals gave informed consent, and the study was conducted according to the Declaration of Helsinki.

Measurement of plasma IFN levels:

Plasma samples were used to measure the levels of IFNs using LEGENDplex Human type 1/2/3 interferon panel (BioLegend #740396), measuring concentrations of IFN-α2, β, γ, λ1, and λ2-3. The assay was performed according to the manufacturers protocol. Samples were acquired on Fortessa (BD Biosciences), and analysis performed in FlowJo 10.8.1 (TreeStar Inc). For analysis samples below the background detection were set to 0 and results reported as the median MFI.

Measurement of plasma cellular activation markers:

Plasma levels of Neopterin (Tecan, Cat# RE59321) and S100A8/A9 (Alarmin/Calprotectin) in plasma were measured using enzyme-linked immunosorbent assay (DuoSet ELISA, R&D Systems, USA; cat number DY8226-05), according to the manufacturer's instructions. Circulating NETs were measured using an MPO-DNA ELISA, with slight modifications from previous descriptions [61, 69]. An anti-MPO antibody (4 µg/ml; clone 4A4, Bio-Rad Laboratories, USA) was used as capture antibody and an anti-dsDNA antibody from the Cell Death Detection ELISA

kit (Roche Diagnostic, Switzerland) was used as detection. Plasma was used at 1:10 dilution in 1% BSA/PBS and incubated for 2 hours at room temperature. The development was done with TMB (BD Biosciences, USA), and the reaction stopped with a 2N sulfuric acid solution. Absorbance was measured at 450 nm and wavelength correction at 540 nm to subtract background using a microplate reader (SpectraMAX 340, USA).

SARS-CoV-2 Antibody and IFN-autoantibody screening:

Plasma samples were measured for the reactivities of antibodies against 14 IFNs (IFNA1, IFNA2, IFNA4, IFNA5, IFNA6, IFNA7, IFNA8, IFNA10, IFNA14, IFNA16, IFNA17, IFNA21, IFNB1, IFNE, IFNG, IFNK, IFNL4, IFNW1, IL28a, IL28b, IL29), cytokines (GM-CSF, IL1F6, IL1RN, IL12, IL17A, IL17F, IL22, IL23, ISG15) and SARS-CoV-2 anti-spike (S1/S2), anti-RBD, anti-Nucleocapsid and Epstein-Barr virus EBNA1 using a broad multiplex bead based array as described previously [70]. Briefly, recombinant proteins were coupled to magnetic beads (MagPlex®, Luminex Corp. Austin, Texas) using AnteoTech Activation Kit for Multiplex Microspheres (Cat# A-LMPAKMM-10) with commercial versions of the proteins (1.5 x 10^6 beads were coupled using 3 micrograms of proteins). One microliter of sample was diluted 1:25 in PBS and later diluted 1:10 in 0.05% PBS with 3% BSA and 5% Milk. The sample dilution was subsequently incubated for two hours with five microliters of the bead solution on a 650 rpm shaker. After three washings in 0.05% PBS, beads were resuspended in 50 microliters of 0.2% PFA during 10 minutes. The secondary antibody (Invitrogen, H10104 lot#2384336) incubation lasted for 30 minutes prior to the final analysis in FlexMap 3D instrument (Luminex Corp). A cut off for positivity was determined by calculating the mean expression + 7SD in the healthy control group.

Neutralization Analysis for Type I Interferon Autoantibodies:

Neutralization assays were performed on samples identified for further analysis based on high ISG scores or elevated responses to type I interferons in a multiplex screening assay (threshold: mean $\pm$ 7 SDs). The assay followed previously reported cell culture-based neutralization protocols [71], utilizing a dual-luciferase reporter system in HEK293T cells to assess the functional inhibition of interferon signaling. On day 1, HEK293T cells in logarithmic growth were detached using 0.01% trypsin, washed, and resuspended at 1×10^6 cells/ml in DMEM (Gibco) supplemented with 10%

FBS and 100 U/ml penicillin-streptomycin. A total of 35,000 cells per well were plated in a 96-well flat-bottom plate. After 3–4 hours of incubation at 37°C to allow for attachment, cells were transfected using Firefly pGL4.45[luc2P/ISRE/Hygro] (IFN-stimulable) and Renilla pRL-SV40 (constitutive control) vectors (Promega) with X-tremeGENE9 transfection reagent (Sigma-Aldrich) at a 3:1 ratio (µl:µg) in OptiMEM medium. The final transfection mix contained 0.8 µg Firefly and 0.4 µg Renilla plasmid per well. Transfection controls were included, and plates were incubated at 37°C for 24 hours. On day 2, stimulation was initiated by adding 5 µl of IFNA2 (100 ng/ml, MedChemExpress) to achieve a final concentration of 10 ng/ml per well, followed immediately by 5 µl of plasma samples (1:10 final dilution in a total 50 µl volume). Non-stimulation controls received media instead of IFNA2, and non-plasma technical controls received media instead of plasma. Positive control samples from APS1 patients (known neutralizing autoantibodies) and negative control blood donor plasma were included. On day 3, following 24 hours of incubation, neutralization was assessed using the Dual-Luciferase Reporter Assay System (Promega). Cells were lysed, and luminescence was measured using a plate reader (Tecan, Magellan) with Firefly (magenta filter) and Renilla (green filter) detection. The Firefly-to-Renilla ratio was calculated, with Renilla readings serving as internal controls to correct for variations in transfection efficiency and cell viability. APS1 patient samples exhibited complete neutralization (>99%, Firefly/Renilla ratio <0.050), while healthy donor samples showed no neutralization (>2.000 ratio). A standard response curve was generated using APS1 samples (0% response) and blood donors (100% response). Definite neutralization was defined as >90% response reduction, while partial neutralization was categorized as 80–90% response reduction. The assay controls performed as expected, confirming the robustness of the neutralization assessment.

Data and preprocessing:

Count table for transcriptomics, olink proteomics data and metabolomics data were retrieved and reanalyzed from Ambikan et al. 2022 [19]. Before analysis, transcriptomics data were filtered for low variance (variance < 0.2) and transformed using variance-stabilizing transformation (VST) from R package Deseq2 [72]. Genes expression profile associated with the Reactome (https://reactome.org) pathways antiviral mechanisms, interferon alpha/beta and interferon gamma were extracted from the data. ISG scores were calculated for each patient by making the sum of genes linked to each pathway. Metabolomics data were transformed in log2 before analysis.

Statistics:

Spearman pairwise correlations between features were done using the R package Hmisc. R package limma for differential abundance analysis was used in metabolomics and proteomics data [73] with adjustment for age, gender and BMI category. R package DESeq2 was used to perform differential gene expression analysis in transcriptomics data [72]. Factors of possible unwanted variation in the data estimated using R package RUVSeq [74] were adjusted along with age, gender and BMI category while executing DESeq2. Means of continuous variables were compared using Mann-Whitney U test. All *p-values* were adjusted using false discovery rate (FDR) and by default FDR < 0.05 was considered significant. Different cutoffs are indicated in the analysis. Absolute fold change higher than 1 was used as a supplementary cutoff in transcriptomics data.

Cell profiling using digital cell quantification (DCQ):

Digital cell quantification (DCQ) was performed to estimate immune cell proportions from bulk RNA sequencing data using the EPIC deconvolution algorithm [27] with a reference signature of 18 blood cell types from the Human Protein Atlas [26]. TPM normalized geneexpression data was used for the analysis. The deconvolution approach utilized a constrained least-squares regression to infer relative immune cell proportions based on predefined reference profiles. To assess the relationship between interferon-stimulated gene (ISG) expression and immune cell distributions, DCQ-derived cell fractions were correlated with ISG scores using Spearman's rank correlation with false discovery rate (FDR) correction for multiple comparisons. All statistical analyses were conducted using R (v4.1.0), with significance thresholds set at FDR < 0.05 unless otherwise specified.

Clustering:

Patient clustering was performed based of interferon simulated genes profile from transcriptomics data using R package ConsensusClusterplus. From 2 to 10 cluster were tested (maxK) on 1000 subsamples (reps), with 0,8 of items (pItem) and all features (pFeature) to sample. The clustering algorithm used was hierarchical clustering (hclust). The number of clusters was determined based on Consensus Cumulative Distribution Function (CDF) and delta area plots.

Visualisation:

Scatter plots, box plots, bubble plots, dot plots, bar plots, PCA plots and volcano plots were done using R packages ggplot2 and ggpubr. Venn diagrams were plotted using R package ggvenn. Heatmaps were done using R package Complexheatmap.

Plasma Treatment of Neutrophils and PBMCs for Monocyte Activation and Flow Cytometry Analysis:

Neutrophils and peripheral blood mononuclear cells (PBMCs) were isolated from buffy-coated blood of healthy donors using density gradient centrifugation with Ficoll-Paque PLUS (GE Healthcare). Whole blood was diluted 1:1 with phosphate-buffered saline (PBS), layered over Ficoll, and centrifuged at 400 × g for 30 min at room temperature without brake. The PBMC layer was collected, washed twice in PBS, and resuspended in RPMI-1640 (Gibco) supplemented with 2 mM L-glutamine and 1% penicillin-streptomycin. Neutrophils were isolated from the erythrocyte pellet via hypotonic lysis, followed by washing and resuspension in RPMI-1640 with 2 mM L-glutamine and 1% penicillin-streptomycin.

PBMCs were seeded in 96-well U-bottom plates at 2×10^5 cells/well, and neutrophils were plated in 96-well flat-bottom plates at 2×10^5 cells/well. Cells were treated with 10% plasma (1:10 dilution in culture medium) from COVID-19 patients stratified by disease severity (mild vs. severe) within the high ISG expression (HIS) group. Control wells received plasma from healthy blood donors (negative control). PBMCs were incubated for 24 hours and neutrophils for 4 hours at 37°C with 5% CO_2.

Following incubation, cells were washed and stained with fluorophore-conjugated antibodies for activation markers. PBMCs were stained for monocyte activation using CD169 (Siglec-1, clone 7-239, BV421; BD Biosciences), a marker induced by type I IFNs, along with CD14 (clone M5E2, PerCP; BioLegend) and HLA-DR (clone L243, PE/Cy7; BioLegend) for monocyte gating. Neutrophil activation was assessed using CD11b (clone ICRF44, PE; BioLegend), CD66b (clone G10F5, FITC; BioLegend) and CD62L (clone DREG-56, BV421; BioLegend). A viability dye (Live/Dead Fixable, Thermo Fisher) was used to exclude dead cells. Samples were acquired on a BD FACSVerse flow cytometer, and data were analyzed using FlowJo v10.

Mean fluorescence intensity (MFI) values for CD169, CD11b, CD66b, and CD62L were compared between treatment groups using Kruskal-Wallis tests followed by Dunn's post-hoc analysis. Correlations between metabolic alterations and immune activation markers were assessed using Spearman's rank correlation with false discovery rate (FDR) correction. Statistical analyses were conducted in GraphPad Prism 9 and R v4.1.0, with significance set at FDR < 0.05 unless otherwise specified.

Acknowledgements:

The authors would like to thank the excellent support received from the study nurses Elisabet Storgard and Ronnie Ask, Södersjukhuset. We thank the National Facility for Autoimmunity and Serology Profiling at SciLifeLab for excellent technical support related to the autoantibody experiments. We also acknowledge Magdalini Lourda, Karolinska Institutet for meaningful discussions that contributed to this work.

Funding:

This work was supported by the Swedish Research Council grants 2021-03035 (S.G.), 2021-00993 (U.N.), 2018-06156 (U.N.), and Center for Medical Innovation grant CIMED-FoUI093304 (S.G.), and received support from Karolinska Institutet Stiftelser och Fonder grant 2022-02232 (S.G.). N.L. acknowledges funding from Swedish Research Council and Göran Gustafsson Foundation, and R.L.J received support from SOF/Stockholm County Council (FoUI-966258).

Authors Contribution:

S.G. Conceptualized the project; S.G., U.N., N.L. and R.L-J., acquired the funding; R.L-J., A.C., S.R., A.Y., S.S.A, X.C., M.S. and M., A.-G., performed research; A.A. and F.M., performed bioinformatic analaysis; H.N. and C.J.T performed clinical research. N.L. and U.N. contributed new reagents/analytic tools; A.A., R.L-J., S.R., A.C., A.Y., F.M., S.S.A, N.L., U.N. and S.G. analyzed data; S.R., A.A., A.Y., R.L-J., A.C., F.M., S.S.A and S.G. wrote the original draft of the paper. A.C., R.L-J., S.R., X.C., M.S., H.N., C.J.T, N.L. and U.N. reviewed and edited the manuscript. All authors have reviewed and approved of the final version..

Figure Legends:

Figure 1: Transcriptomic analysis of HC (*n=21*), convalescence (*n=10*), mild (*n=28*) or severe (*n=11*) COVID-19 patients. A) Schematic figure showing the clinical characteristics of COVID-19 infected individuals. **B)** Heatmap of the interferon (IFN) stimulated genes (ISG) profile of the clinical cohort from transcriptomic data. **C)** Boxplots of the ISG score for type I ISGs, type II ISGs, and antiviral ISGs in the clinical groups separately. **D)** Plasma levels of IFN-λ1, IFN-λ2/3, IFN-γ, IFN-β, and IFN-α2 measured by LEGENDplex assay expressed as Median Fluorescent Intensity (MFI). Statistical significance was measured using Kruskal-Wallis test by ANOVA with significance * $p<0.05$, ** $p<0.01$, *** $p<0.001$, and **** $p<0.0001$.

Figure 2: Clustering of COVID-19 patients based on ISG transcriptomic profiles and detection of IFN autoantibodies. A) Heatmap of the consensus clustering matrix depicting patient clustering based on ISG expression. Patients are displayed along both rows and columns, with clinical conditions (top) and ISG-based clusters (bottom) indicated. Consensus values range from 0 (no co-clustering) to 1 (consistent co-clustering) and are color-coded from white to red. **B)** Bar plot showing the distribution of clinically categorized subjects within each ISG-defined cluster (low-ISG: LIS, moderate-ISG: MIS, and high-ISG: HIS). **C)** Box plots illustrating the antiviral, type-I IFN, and type-II IFN ISG scores across different ISG-defined clusters, highlighting differential ISG expression patterns. **D)** Heatmap showing host IFN autoantibody expression across patient clusters. Antibodies detected above the threshold (mean fluorescence intensity of healthy controls + 7 SD) are marked with red stars. The bottom row displays the results of the IFN-I autoantibody neutralization assay for the corresponding samples wherever performed. Clinical metadata, including patient condition, ISG-based cluster, gender, age, and BMI, are displayed above the heatmap. **E)** Dot plots representing the Log_{10} fluorescence intensity of antibodies against SARS-CoV-2 nucleocapsid, receptor-binding domain (RBD), and spike protein across the ISG-defined clusters. The horizontal line indicates the detection threshold (mean fluorescence intensity of healthy controls + 7 SD) for SARS-CoV-2-specific autoantibodies.

Figure 3: Multi-omics analysis of inflammatory and metabolic perturbations across ISG-defined clusters. A) Principal Component Analysis (PCA) plot of Olink proteomic data from healthy controls (HC), convalescent individuals (Conv), and COVID-19 patients stratified into LIS, MIS, and HIS clusters. The first two principal components are displayed, with variance explained indicated on the axes and color-coded cluster categories. **B)** Heatmap of significantly differentially expressed proteins across ISG-defined clusters (LIS, MIS, HIS). Protein expression values are z-score transformed, with hierarchical clustering of patients. Metadata including cluster, age, gender, and BMI is annotated on the top. **C)** PCA plot of metabolomic data from HC, Conv, and COVID-19 patients categorized into LIS, MIS, and HIS clusters. The first two principal components are shown, color-coded by cluster categories, highlighting metabolic differences across groups. **D)** UpSet plot depicting the overlap of significantly altered metabolites across ISG-defined clusters (LIS, MIS, HIS). The number of differentially abundant metabolites (LIMMA, FDR < 0.05) in each comparison is indicated, highlighting shared and unique metabolic disruptions across clusters. **E)** Heatmap of significantly altered metabolites between LIS, MIS, and HIS clusters. Metabolite abundance is log2 transformed and z-score normalized, with hierarchical clustering applied. Row annotation represents metabolite super-pathways, while column annotations indicate sample clusters.

Figure 4: Innate immune activation and association with ISG expression in COVID-19 clusters. A) Stacked bar plot showing the proportion of immune cell types identified from whole-blood transcriptomics data using Digital Cytometry Quantification (DCQ) across healthy controls (HC), convalescent individuals (Conv), and ISG-defined clusters (LIS, MIS, HIS). Cell types with a frequency < 0.05 were grouped under "other cells." **B-D)** Boxplots depicting plasma levels of key immune activation markers: (B) S100A8/A9 (ng/mL), (C) Neopterin (nMol/mL), and (D) MPO:DNA complexes (% of total), indicative of NETosis, across ISG clusters. *p*-values were calculated using the Kruskal-Wallis test, with significance denoted as **p*<0.05, ***p*<0.01, ****p*<0.001, and *****p*<0.0001. **E)** Bar plot displaying the correlation coefficients between GSVA enrichment scores of immune cell types and ISG expression scores in each cluster. Significant correlations (Spearman correlation, *p*-value < 0.05) highlight the association between specific immune cell populations and the interferon response.

Figure 5: Immune and metabolic determinants of severity in the HIS cluster. A) Boxplots showing the differential ability of plasma from mild and severe HIS cases to activate healthy neutrophils and monocytes in an ex vivo assay. Activation was assessed using CD66b/CD11b for neutrophils and CD169 for monocytes. Lower activation in severe cases suggests the presence of suppressive soluble factors in circulation. **B)** Boxplots showing the plasma levels of key inflammatory mediators HGF, MCP-3 (CCL7), and IL-6, which were significantly elevated in severe HIS cases. Adjusted *p*-values were calculated using LIMMA, with significance thresholds: * *p*<0.05, ** *p*<0.01 and *** *p*<0.001. **C)** Heatmap of $\log_2$-scaled and Z-score transformed metabolite levels significantly altered between mild and severe HIS cases. Xenobiotics were excluded. Rows represent super-pathways of metabolites, and columns represent individual HIS patient samples. **D)** Heatmap showing Spearman correlation coefficients between significantly altered metabolites and neutrophil (CD66b, CD11b) and monocyte (CD169) activation markers in HIS patients. *p*-values < 0.05 were considered statistically significant.

References:

1. Parasher A: **COVID-19: Current understanding of its Pathophysiology, Clinical presentation and Treatment**. *Postgraduate medical journal* 2021, **97**(1147):312-320.
2. Fara A, Mitrev Z, Rosalia RA, Assas BM: **Cytokine storm and COVID-19: a chronicle of pro-inflammatory cytokines**. *Open biology* 2020, **10**(9):200160.
3. Swiecki M, Colonna M: **Type I interferons: diversity of sources, production pathways and effects on immune responses**. *Current opinion in virology* 2011, **1**(6):463-475.
4. Kim YM, Shin EC: **Type I and III interferon responses in SARS-CoV-2 infection**. *Experimental & molecular medicine* 2021, **53**(5):750-760.
5. Pervolaraki K, Rastgou Talemi S, Albrecht D, Bormann F, Bamford C, Mendoza JL, Garcia KC, McLauchlan J, Höfer T, Stanifer ML *et al*: **Differential induction of interferon stimulated genes between type I and type III interferons is independent of interferon receptor abundance**. *PLoS pathogens* 2018, **14**(11):e1007420.
6. Park A, Iwasaki A: **Type I and Type III Interferons - Induction, Signaling, Evasion, and Application to Combat COVID-19**. *Cell host & microbe* 2020, **27**(6):870-878.
7. Decker T: **The early interferon catches the SARS-CoV-2**. *The Journal of experimental medicine* 2021, **218**(10).
8. Zhang Q, Bastard P, Liu Z, Le Pen J, Moncada-Velez M, Chen J, Ogishi M, Sabli IKD, Hodeib S, Korol C *et al*: **Inborn errors of type I IFN immunity in patients with life-threatening COVID-19**. *Science (New York, NY)* 2020, **370**(6515).
9. Bastard P, Rosen LB, Zhang Q, Michailidis E, Hoffmann HH, Zhang Y, Dorgham K, Philippot Q, Rosain J, Béziat V *et al*: **Autoantibodies against type I IFNs in patients with life-threatening COVID-19**. *Science (New York, NY)* 2020, **370**(6515).
10. Smith N, Possémé C, Bondet V, Sugrue J, Townsend L, Charbit B, Rouilly V, Saint-André V, Dott T, Pozo AR *et al*: **Defective activation and regulation of type I interferon immunity is associated with increasing COVID-19 severity**. *Nature communications* 2022, **13**(1):7254.
11. Zhu L, Yang P, Zhao Y, Zhuang Z, Wang Z, Song R, Zhang J, Liu C, Gao Q, Xu Q *et al*: **Single-Cell Sequencing of Peripheral Mononuclear Cells Reveals Distinct Immune Response Landscapes of COVID-19 and Influenza Patients**. *Immunity* 2020, **53**(3):685-696 e683.
12. Acharya D, Liu G, Gack MU: **Dysregulation of type I interferon responses in COVID-19**. *Nature reviews Immunology* 2020, **20**(7):397-398.
13. Fritsch SD, Weichhart T: **Effects of Interferons and Viruses on Metabolism**. *Frontiers in immunology* 2016, **7**:630.
14. Crow MK, Ronnblom L: **Type I interferons in host defence and inflammatory diseases**. *Lupus science & medicine* 2019, **6**(1):e000336.
15. Wang X, Tang Q, Li H, Jiang H, Xu J, Bergquist R, Qin Z: **Autoantibodies against type I interferons in COVID-19 infection: A systematic review and meta-analysis**. *International journal of infectious diseases : IJID : official publication of the International Society for Infectious Diseases* 2023, **130**:147-152.
16. Peluso MJ, Deeks SG: **Mechanisms of long COVID and the path toward therapeutics**. *Cell* 2024, **187**(20):5500-5529.

17. Chen Y, Lin Q, Cheng H, Xiang Q, Zhou W, Wu J, Wang X: **Immunometabolic shifts in autoimmune disease: Mechanisms and pathophysiological implications**. *Autoimmunity reviews* 2025, **24**(3):103738.
18. Chen X, Saccon E, Appelberg KS, Mikaeloff F, Rodriguez JE, Vinhas BS, Frisan T, Végvári Á, Mirazimi A, Neogi U *et al*: **Type-I interferon signatures in SARS-CoV-2 infected Huh7 cells**. *Cell death discovery* 2021, **7**(1):114.
19. Ambikan AT, Yang H, Krishnan S, Svensson Akusjärvi S, Gupta S, Lourda M, Sperk M, Arif M, Zhang C, Nordqvist H *et al*: **Multi-omics personalized network analyses highlight progressive disruption of central metabolism associated with COVID-19 severity**. *Cell systems* 2022, **13**(8):665-681 e664.
20. Carrau L, Frere JJ, Golynker I, Fajardo A, Rivera CF, Horiuchi S, Roonprapunt T, Minkoff JM, Blanco-Melo D, TenOever B: **Delayed engagement of host defenses enables SARS-CoV-2 viremia and productive infection of distal organs in the hamster model of COVID-19**. *Science signaling* 2023, **16**(789):eadg5470.
21. Krishnan S, Nordqvist H, Ambikan AT, Gupta S, Sperk M, Svensson-Akusjärvi S, Mikaeloff F, Benfeitas R, Saccon E, Ponnan SM *et al*: **Metabolic Perturbation Associated With COVID-19 Disease Severity and SARS-CoV-2 Replication**. *Molecular & cellular proteomics : MCP* 2021, **20**:100159.
22. York AG, Williams KJ, Argus JP, Zhou QD, Brar G, Vergnes L, Gray EE, Zhen A, Wu NC, Yamada DH *et al*: **Limiting Cholesterol Biosynthetic Flux Spontaneously Engages Type I IFN Signaling**. *Cell* 2015, **163**(7):1716-1729.
23. Wang Y, Wang Y, Ding L, Ren X, Wang B, Wang L, Zhao S, Yue X, Wu Z, Li C *et al*: **Tim-4 reprograms cholesterol metabolism to suppress antiviral innate immunity by disturbing the Insig1-SCAP interaction in macrophages**. *Cell reports* 2022, **41**(9):111738.
24. Wu D, Sanin DE, Everts B, Chen Q, Qiu J, Buck MD, Patterson A, Smith AM, Chang CH, Liu Z *et al*: **Type 1 Interferons Induce Changes in Core Metabolism that Are Critical for Immune Function**. *Immunity* 2016, **44**(6):1325-1336.
25. Ebrahimi KH, Gilbert-Jaramillo J, James WS, McCullagh JSO: **Interferon-stimulated gene products as regulators of central carbon metabolism**. *The FEBS journal* 2021, **288**(12):3715-3726.
26. Uhlen M, Karlsson MJ, Zhong W, Tebani A, Pou C, Mikes J, Lakshmikanth T, Forsström B, Edfors F, Odeberg J *et al*: **A genome-wide transcriptomic analysis of protein-coding genes in human blood cells**. *Science (New York, NY)* 2019, **366**(6472).
27. Racle J, Gfeller D: **EPIC: A Tool to Estimate the Proportions of Different Cell Types from Bulk Gene Expression Data**. *Methods in molecular biology (Clifton, NJ)* 2020, **2120**:233-248.
28. Mantovani A, Cassatella MA, Costantini C, Jaillon S: **Neutrophils in the activation and regulation of innate and adaptive immunity**. *Nature reviews Immunology* 2011, **11**(8):519-531.
29. Xia P, Ji X, Yan L, Lian S, Chen Z, Luo Y: **Roles of S100A8, S100A9 and S100A12 in infection, inflammation and immunity**. *Immunology* 2024, **171**(3):365-376.
30. Guo Q, Zhao Y, Li J, Liu J, Yang X, Guo X, Kuang M, Xia H, Zhang Z, Cao L *et al*: **Induction of alarmin S100A8/A9 mediates activation of aberrant neutrophils in the pathogenesis of COVID-19**. *Cell host & microbe* 2021, **29**(2):222-235 e224.

31. Apel F, Andreeva L, Knackstedt LS, Streeck R, Frese CK, Goosmann C, Hopfner KP, Zychlinsky A: **The cytosolic DNA sensor cGAS recognizes neutrophil extracellular traps**. *Science signaling* 2021, **14**(673).
32. Connelly AN, Huijbregts RPH, Pal HC, Kuznetsova V, Davis MD, Ong KL, Fay CX, Greene ME, Overton ET, Hel Z: **Optimization of methods for the accurate characterization of whole blood neutrophils**. *Scientific reports* 2022, **12**(1):3667.
33. Affandi AJ, Olesek K, Grabowska J, Nijen Twilhaar MK, Rodríguez E, Saris A, Zwart ES, Nossent EJ, Kalay H, de Kok M *et al*: **CD169 Defines Activated CD14(+) Monocytes With Enhanced CD8(+) T Cell Activation Capacity**. *Frontiers in immunology* 2021, **12**:697840.
34. Tsou CL, Peters W, Si Y, Slaymaker S, Aslanian AM, Weisberg SP, Mack M, Charo IF: **Critical roles for CCR2 and MCP-3 in monocyte mobilization from bone marrow and recruitment to inflammatory sites**. *The Journal of clinical investigation* 2007, **117**(4):902-909.
35. Perreau M, Suffiotti M, Marques-Vidal P, Wiedemann A, Levy Y, Laouénan C, Ghosn J, Fenwick C, Comte D, Roger T *et al*: **The cytokines HGF and CXCL13 predict the severity and the mortality in COVID-19 patients**. *Nature communications* 2021, **12**(1):4888.
36. Hafez W, Nasa P, Khairy A, Jose M, Abdelshakour M, Ahmed S, Abdulaal F, Nair N, Ahmad M, Rashid VJ *et al*: **Interleukin-6 and the determinants of severe COVID-19: A retrospective cohort study**. *Medicine* 2023, **102**(45):e36037.
37. Angajala A, Lim S, Phillips JB, Kim JH, Yates C, You Z, Tan M: **Diverse Roles of Mitochondria in Immune Responses: Novel Insights Into Immuno-Metabolism**. *Frontiers in immunology* 2018, **9**:1605.
38. Wallner S, Orsó E, Grandl M, Konovalova T, Liebisch G, Schmitz G: **Phosphatidylcholine and phosphatidylethanolamine plasmalogens in lipid loaded human macrophages**. *PloS one* 2018, **13**(10):e0205706.
39. Lee M, Lee SY, Bae YS: **Functional roles of sphingolipids in immunity and their implication in disease**. *Experimental & molecular medicine* 2023, **55**(6):1110-1130.
40. Knight JS, Caricchio R, Casanova JL, Combes AJ, Diamond B, Fox SE, Hanauer DA, James JA, Kanthi Y, Ladd V *et al*: **The intersection of COVID-19 and autoimmunity**. *The Journal of clinical investigation* 2021, **131**(24).
41. Eskandarian Boroujeni M, Sekrecka A, Antonczyk A, Hassani S, Sekrecki M, Nowicka H, Lopacinska N, Olya A, Kluzek K, Wesoly J *et al*: **Dysregulated Interferon Response and Immune Hyperactivation in Severe COVID-19: Targeting STATs as a Novel Therapeutic Strategy**. *Frontiers in immunology* 2022, **13**:888897.
42. Galbraith MD, Kinning KT, Sullivan KD, Araya P, Smith KP, Granrath RE, Shaw JR, Baxter R, Jordan KR, Russell S *et al*: **Specialized interferon action in COVID-19**. *Proceedings of the National Academy of Sciences of the United States of America* 2022, **119**(11).
43. da Silva RP, Gonçalves JIB, Zanin RF, Schuch FB, de Souza APD: **Circulating Type I Interferon Levels and COVID-19 Severity: A Systematic Review and Meta-Analysis**. *Frontiers in immunology* 2021, **12**:657363.
44. Wilk AJ, Rustagi A, Zhao NQ, Roque J, Martínez-Colón GJ, McKechnie JL, Ivison GT, Ranganath T, Vergara R, Hollis T *et al*: **A single-cell atlas of the peripheral immune response in patients with severe COVID-19**. *Nature medicine* 2020, **26**(7):1070-1076.

45. Lee JS, Park S, Jeong HW, Ahn JY, Choi SJ, Lee H, Choi B, Nam SK, Sa M, Kwon JS *et al*: **Immunophenotyping of COVID-19 and influenza highlights the role of type I interferons in development of severe COVID-19**. *Science immunology* 2020, **5**(49).
46. Zhou Z, Ren L, Zhang L, Zhong J, Xiao Y, Jia Z, Guo L, Yang J, Wang C, Jiang S *et al*: **Heightened Innate Immune Responses in the Respiratory Tract of COVID-19 Patients**. *Cell host & microbe* 2020, **27**(6):883-890 e882.
47. Daman AW, Josefowicz SZ: **Epigenetic and transcriptional control of interferon-β**. *The Journal of experimental medicine* 2021, **218**(9).
48. Lee JS, Shin EC: **The type I interferon response in COVID-19: implications for treatment**. *Nature reviews Immunology* 2020, **20**(10):585-586.
49. Znaidia M, Demeret C, van der Werf S, Komarova AV: **Characterization of SARS-CoV-2 Evasion: Interferon Pathway and Therapeutic Options**. *Viruses* 2022, **14**(6).
50. Chiale C, Greene TT, Zuniga EI: **Interferon induction, evasion, and paradoxical roles during SARS-CoV-2 infection**. *Immunological reviews* 2022, **309**(1):12-24.
51. Kisand K, Link M, Wolff AS, Meager A, Tserel L, Org T, Murumägi A, Uibo R, Willcox N, Trebusak Podkrajsek K *et al*: **Interferon autoantibodies associated with AIRE deficiency decrease the expression of IFN-stimulated genes**. *Blood* 2008, **112**(7):2657-2666.
52. Bastard P, Gervais A, Le Voyer T, Rosain J, Philippot Q, Manry J, Michailidis E, Hoffmann HH, Eto S, Garcia-Prat M *et al*: **Autoantibodies neutralizing type I IFNs are present in ~4% of uninfected individuals over 70 years old and account for ~20% of COVID-19 deaths**. *Science immunology* 2021, **6**(62).
53. Porcelijn L, Schmidt DE, Oldert G, Hofstede-van Egmond S, Kapur R, Zwaginga JJ, de Haas M: **Evolution and Utility of Antiplatelet Autoantibody Testing in Patients with Immune Thrombocytopenia**. *Transfusion medicine reviews* 2020, **34**(4):258-269.
54. Vazquez SE, Mann SA, Bodansky A, Kung AF, Quandt Z, Ferré EMN, Landegren N, Eriksson D, Bastard P, Zhang SY *et al*: **Autoantibody discovery across monogenic, acquired, and COVID-19-associated autoimmunity with scalable PhIP-seq**. *eLife* 2022, **11**.
55. Galani IE, Rovina N, Lampropoulou V, Triantafyllia V, Manioudaki M, Pavlos E, Koukaki E, Fragkou PC, Panou V, Rapti V *et al*: **Untuned antiviral immunity in COVID-19 revealed by temporal type I/III interferon patterns and flu comparison**. *Nature immunology* 2021, **22**(1):32-40.
56. Mellett L, Khader SA: **S100A8/A9 in COVID-19 pathogenesis: Impact on clinical outcomes**. *Cytokine & growth factor reviews* 2022, **63**:90-97.
57. Chauvin M, Larsen M, Quirant B, Quentric P, Dorgham K, Royer L, Vallet H, Guihot A, Combadière B, Combadière C *et al*: **Elevated Neopterin Levels Predict Fatal Outcome in SARS-CoV-2-Infected Patients**. *Frontiers in cellular and infection microbiology* 2021, **11**:709893.
58. Cho SD, Shin H, Kim S, Kim HJ: **Insights on interferon-independent induction of interferon-stimulated genes shaping the lung's response in early SARS-CoV-2 infection**. *Heliyon* 2023, **9**(12):e22997.
59. Wang W, Xu L, Su J, Peppelenbosch MP, Pan Q: **Transcriptional Regulation of Antiviral Interferon-Stimulated Genes**. *Trends in microbiology* 2017, **25**(7):573-584.

60. Ackermann M, Anders HJ, Bilyy R, Bowlin GL, Daniel C, De Lorenzo R, Egeblad M, Henneck T, Hidalgo A, Hoffmann M *et al*: **Patients with COVID-19: in the dark-NETs of neutrophils**. *Cell death and differentiation* 2021, **28**(11):3125-3139.
61. Zuo Y, Yalavarthi S, Shi H, Gockman K, Zuo M, Madison JA, Blair C, Weber A, Barnes BJ, Egeblad M *et al*: **Neutrophil extracellular traps in COVID-19**. *JCI insight* 2020, **5**(11).
62. Palmer CS: **Innate metabolic responses against viral infections**. *Nature metabolism* 2022, **4**(10):1245-1259.
63. Masoodi M, Peschka M, Schmiedel S, Haddad M, Frye M, Maas C, Lohse A, Huber S, Kirchhof P, Nofer JR *et al*: **Disturbed lipid and amino acid metabolisms in COVID-19 patients**. *Journal of molecular medicine (Berlin, Germany)* 2022, **100**(4):555-568.
64. Wu D, Shu T, Yang X, Song JX, Zhang M, Yao C, Liu W, Huang M, Yu Y, Yang Q *et al*: **Plasma metabolomic and lipidomic alterations associated with COVID-19**. *National science review* 2020, **7**(7):1157-1168.
65. Lai M, De Carli A, Filipponi C, Iacono E, La Rocca V, Lottini G, Piazza CR, Quaranta P, Sidoti M, Pistello M *et al*: **Lipid balance remodelling by human positive-strand RNA viruses and the contribution of lysosomes**. *Antiviral research* 2022, **206**:105398.
66. Icard P, Lincet H, Wu Z, Coquerel A, Forgez P, Alifano M, Fournel L: **The key role of Warburg effect in SARS-CoV-2 replication and associated inflammatory response**. *Biochimie* 2021, **180**:169-177.
67. Peace CG, O'Neill LA: **The role of itaconate in host defense and inflammation**. *The Journal of clinical investigation* 2022, **132**(2).
68. Sánchez-García FJ, Pérez-Hernández CA, Rodríguez-Murillo M, Moreno-Altamirano MMB: **The Role of Tricarboxylic Acid Cycle Metabolites in Viral Infections**. *Frontiers in cellular and infection microbiology* 2021, **11**:725043.
69. Vedder D, Gerritsen M, Nurmohamed MT, van Vollenhoven RF, Lood C: **A neutrophil signature is strongly associated with increased cardiovascular risk in gout**. *Rheumatology (Oxford, England)* 2021, **60**(6):2783-2790.
70. Le Voyer T, Parent AV, Liu X, Cederholm A, Gervais A, Rosain J, Nguyen T, Perez Lorenzo M, Rackaityte E, Rinchai D *et al*: **Autoantibodies against type I IFNs in humans with alternative NF-κB pathway deficiency**. *Nature* 2023, **623**(7988):803-813.
71. Arrestier R, Bastard P, Belmondo T, Voiriot G, Urbina T, Luyt CE, Gervais A, Bizien L, Segaux L, Ben Ahmed M *et al*: **Auto-antibodies against type I IFNs in > 10% of critically ill COVID-19 patients: a prospective multicentre study**. *Ann Intensive Care* 2022, **12**(1):121.
72. Love MI, Huber W, Anders S: **Moderated estimation of fold change and dispersion for RNA-seq data with DESeq2**. *Genome biology* 2014, **15**(12):550.
73. Ritchie ME, Phipson B, Wu D, Hu Y, Law CW, Shi W, Smyth GK: **limma powers differential expression analyses for RNA-sequencing and microarray studies**. *Nucleic acids research* 2015, **43**(7):e47.
74. Risso D, Ngai J, Speed TP, Dudoit S: **Normalization of RNA-seq data using factor analysis of control genes or samples**. *Nature biotechnology* 2014, **32**(9):896-902.

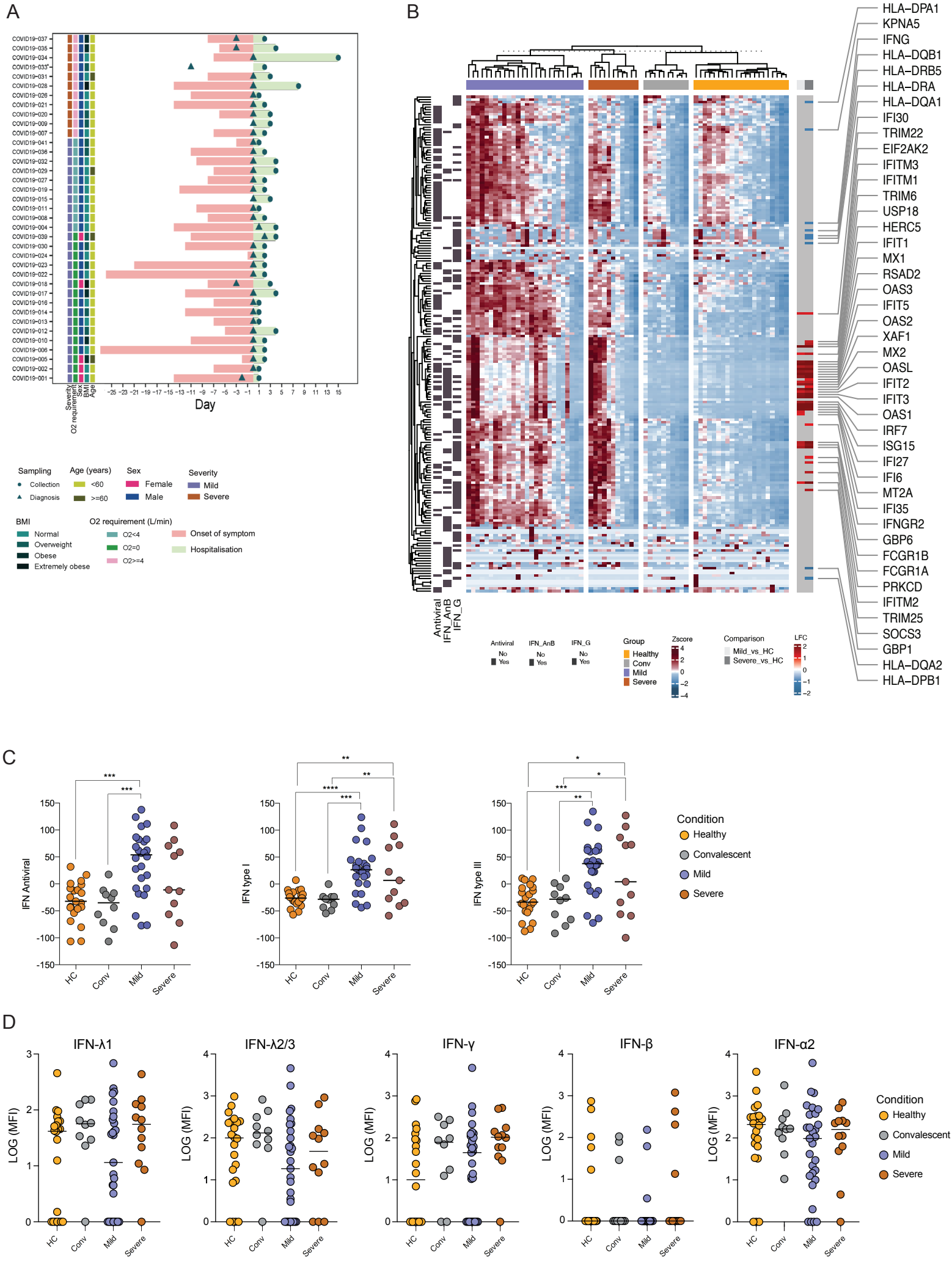
A
Day
Severity
O2 requirement
Sex
BMI
Age
Sampling
Collection
Diagnosis
Age (years)
<60
>=60
Sex
Female
Male
Severity
Mild
Severe
BMI
Normal
Overweight
Obese
Extremely obese
O2 requirement (L/min)
O2<4
O2=0
O2>=4
Onset of symptom
Hospitalisation
B
HLA-DPA1
KPNA5
IFNG
HLA-DQB1
HLA-DRB5
HLA-DRA
HLA-DQA1
IFI30
TRIM22
EIF2AK2
IFITM3
IFITM1
TRIM6
USP18
HERC5
IFIT1
MX1
RSAD2
OAS3
IFIT5
OAS2
XAF1
MX2
OASL
IFIT2
IFIT3
OAS1
IRF7
ISG15
IFI27
IFI6
MT2A
IFI35
IFNGR2
GBP6
FCGR1B
FCGR1A
PRKCD
IFITM2
TRIM25
SOCS3
GBP1
HLA-DQA2
HLA-DPB1
Antiviral
IFN_AnB
IFN_G
Group
Healthy
Conv
Mild
Severe
Zscore
Comparison
Mild_vs_HC
Severe_vs_HC
LFC
C
IFN Antiviral
IFN type I
IFN type III
HC
Conv
Mild
Severe
Condition
Healthy
Convalescent
Mild
Severe
D
IFN-λ1
IFN-λ2/3
IFN-γ
IFN-β
IFN-α2
LOG (MFI)
HC
Conv
Mild
Severe
Condition
Healthy
Convalescent
Mild
Severe

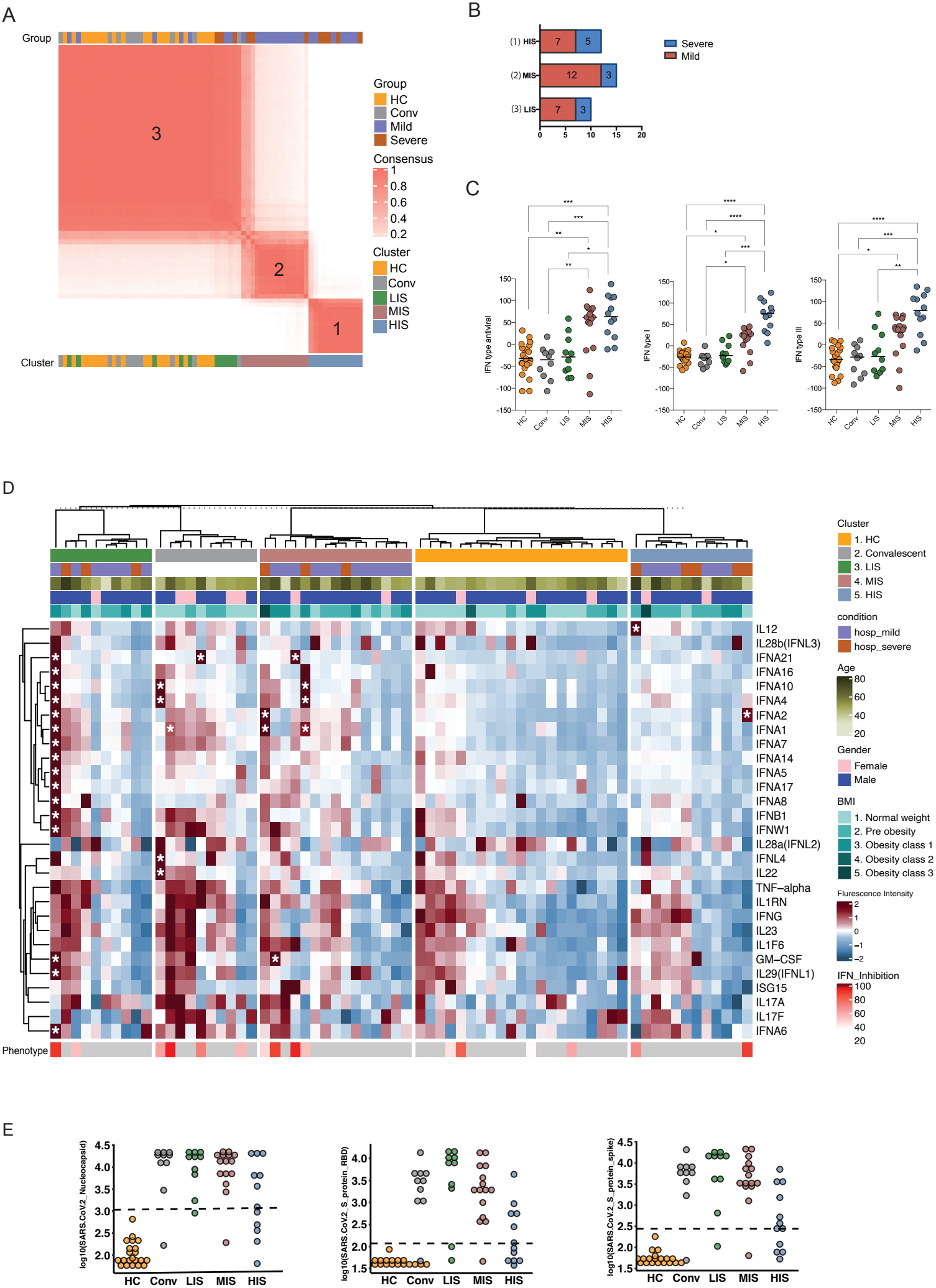
A
Group
Cluster
3
2
1
Group
HC
Conv
Mild
Severe
Consensus
1
0.8
0.6
0.4
0.2
Cluster
HC
Conv
LIS
MIS
HIS
B
(1) HIS
(2) MIS
(3) LIS
7
5
12
3
7
3
0
5
10
15
20
Severe
Mild
C
IFN type antiviral
IFN type I
IFN type III
HC
Conv
LIS
MIS
HIS
D
Cluster
1. HC
2. Convalescent
3. LIS
4. MIS
5. HIS
condition
hosp_mild
hosp_severe
Age
80
60
40
20
Gender
Female
Male
BMI
1. Normal weight
2. Pre obesity
3. Obesity class 1
4. Obesity class 2
5. Obesity class 3
Flurescence Intensity
2
1
0
−1
−2
IFN_Inhibition
100
80
60
40
20
IL12
IL28b(IFNL3)
IFNA21
IFNA16
IFNA10
IFNA4
IFNA2
IFNA1
IFNA7
IFNA14
IFNA5
IFNA17
IFNA8
IFNB1
IFNW1
IL28a(IFNL2)
IFNL4
IL22
TNF−alpha
IL1RN
IFNG
IL23
IL1F6
GM−CSF
IL29(IFNL1)
ISG15
IL17A
IL17F
IFNA6
Phenotype
E
log10(SARS.CoV2_Nucleocapsid)
log10(SARS.CoV2_S_protein_RBD)
log10(SARS.CoV2_S_protein_spike)
HC
Conv
LIS
MIS
HIS

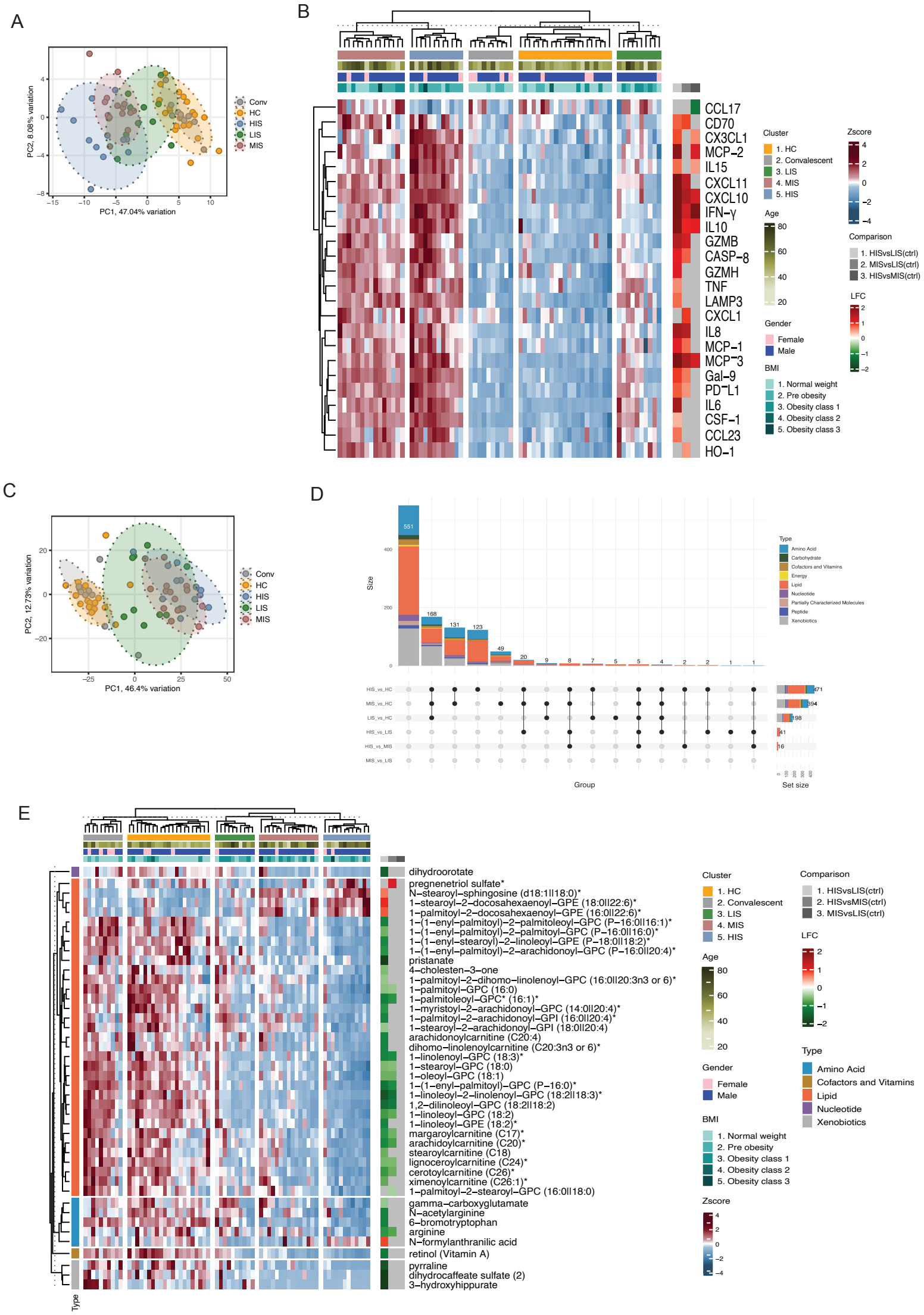
A
PC2, 8.08% variation
PC1, 47.04% variation
Conv
HC
HIS
LIS
MIS
B
CCL17
CD70
CX3CL1
MCP-2
IL15
CXCL11
CXCL10
IFN-γ
IL10
GZMB
CASP-8
GZMH
TNF
LAMP3
CXCL1
IL8
MCP-1
MCP-3
Gal-9
PD-L1
IL6
CSF-1
CCL23
HO-1
Cluster
1. HC
2. Convalescent
3. LIS
4. MIS
5. HIS
Age
Gender
Female
Male
BMI
1. Normal weight
2. Pre obesity
3. Obesity class 1
4. Obesity class 2
5. Obesity class 3
Zscore
Comparison
1. HISvsLIS(ctrl)
2. MISvsLIS(ctrl)
3. HISvsMIS(ctrl)
LFC
C
PC2, 12.73% variation
PC1, 46.4% variation
Conv
HC
HIS
LIS
MIS
D
Size
Type
Amino Acid
Carbohydrate
Cofactors and Vitamins
Energy
Lipid
Nucleotide
Partially Characterized Molecules
Peptide
Xenobiotics
HIS_vs_HC
MIS_vs_HC
LIS_vs_HC
HIS_vs_LIS
HIS_vs_MIS
MIS_vs_LIS
Group
Set size
E
dihydroorotate
pregnenetriol sulfate*
N-stearoyl-sphingosine (d18:1|18:0)*
1-stearoyl-2-docosahexaenoyl-GPE (18:0|22:6)*
1-palmitoyl-2-docosahexaenoyl-GPE (16:0|22:6)*
1-(1-enyl-palmitoyl)-2-palmitoleoyl-GPC (P-16:0|16:1)*
1-(1-enyl-palmitoyl)-2-palmitoyl-GPC (P-16:0|16:0)*
1-(1-enyl-stearoyl)-2-linoleoyl-GPE (P-18:0|18:2)*
1-(1-enyl-palmitoyl)-2-arachidonoyl-GPC (P-16:0|20:4)*
pristanate
4-cholesten-3-one
1-palmitoyl-2-dihomo-linolenoyl-GPC (16:0|20:3n3 or 6)*
1-palmitoyl-GPC (16:0)
1-palmitoleoyl-GPC* (16:1)*
1-myristoyl-2-arachidonoyl-GPC (14:0|20:4)*
1-palmitoyl-2-arachidonoyl-GPI (16:0|20:4)*
1-stearoyl-2-arachidonoyl-GPI (18:0|20:4)
arachidonoylcarnitine (C20:4)
dihomo-linolenoylcarnitine (C20:3n3 or 6)*
1-linolenoyl-GPC (18:3)*
1-stearoyl-GPC (18:0)
1-oleoyl-GPC (18:1)
1-(1-enyl-palmitoyl)-GPC (P-16:0)*
1-linoleoyl-2-linolenoyl-GPC (18:2|18:3)*
1,2-dilinoleoyl-GPC (18:2|18:2)
1-linoleoyl-GPC (18:2)
1-linoleoyl-GPE (18:2)*
margaroylcarnitine (C17)*
arachidoylcarnitine (C20)*
stearoylcarnitine (C18)
lignoceroylcarnitine (C24)*
cerotoylcarnitine (C26)*
ximenoylcarnitine (C26:1)*
1-palmitoyl-2-stearoyl-GPC (16:0|18:0)
gamma-carboxyglutamate
N-acetylarginine
6-bromotryptophan
arginine
N-formylanthranilic acid
retinol (Vitamin A)
pyrraline
dihydrocaffeate sulfate (2)
3-hydroxyhippurate
Type
Cluster
1. HC
2. Convalescent
3. LIS
4. MIS
5. HIS
Age
Gender
Female
Male
BMI
1. Normal weight
2. Pre obesity
3. Obesity class 1
4. Obesity class 2
5. Obesity class 3
Zscore
Comparison
1. HISvsLIS(ctrl)
2. HISvsMIS(ctrl)
3. MISvsLIS(ctrl)
LFC
Type
Amino Acid
Cofactors and Vitamins
Lipid
Nucleotide
Xenobiotics

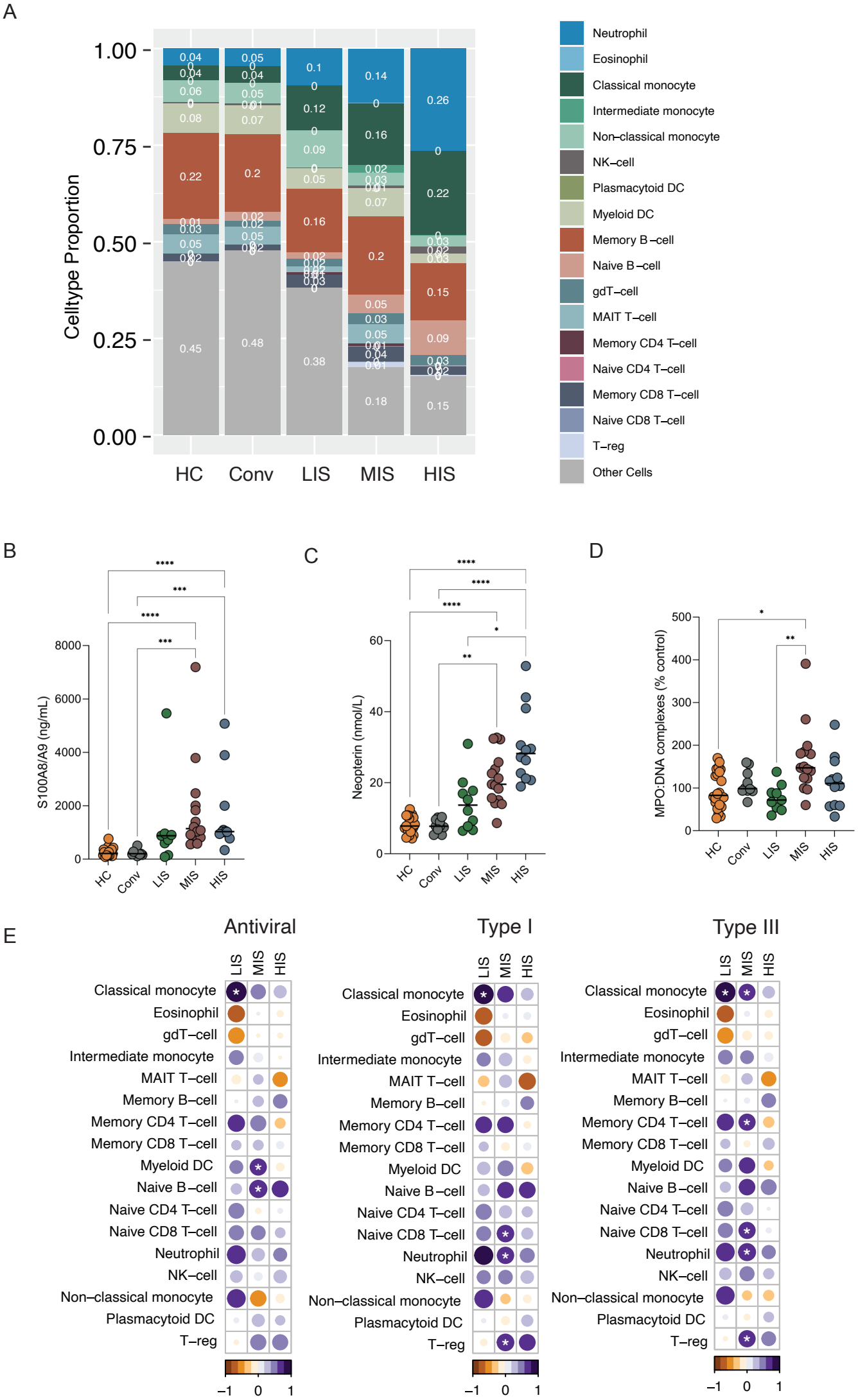
A
Celltype Proportion
1.00
0.75
0.50
0.25
0.00
HC
Conv
LIS
MIS
HIS
Neutrophil
Eosinophil
Classical monocyte
Intermediate monocyte
Non–classical monocyte
NK–cell
Plasmacytoid DC
Myeloid DC
Memory B–cell
Naive B–cell
gdT–cell
MAIT T–cell
Memory CD4 T–cell
Naive CD4 T–cell
Memory CD8 T–cell
Naive CD8 T–cell
T–reg
Other Cells
B
S100A8/A9 (ng/mL)
C
Neopterin (nmol/L)
D
MPO:DNA complexes (% control)
E
Antiviral
Type I
Type III
LIS
MIS
HIS
Classical monocyte
Eosinophil
gdT–cell
Intermediate monocyte
MAIT T–cell
Memory B–cell
Memory CD4 T–cell
Memory CD8 T–cell
Myeloid DC
Naive B–cell
Naive CD4 T–cell
Naive CD8 T–cell
Neutrophil
NK–cell
Non–classical monocyte
Plasmacytoid DC
T–reg
–1
0
1

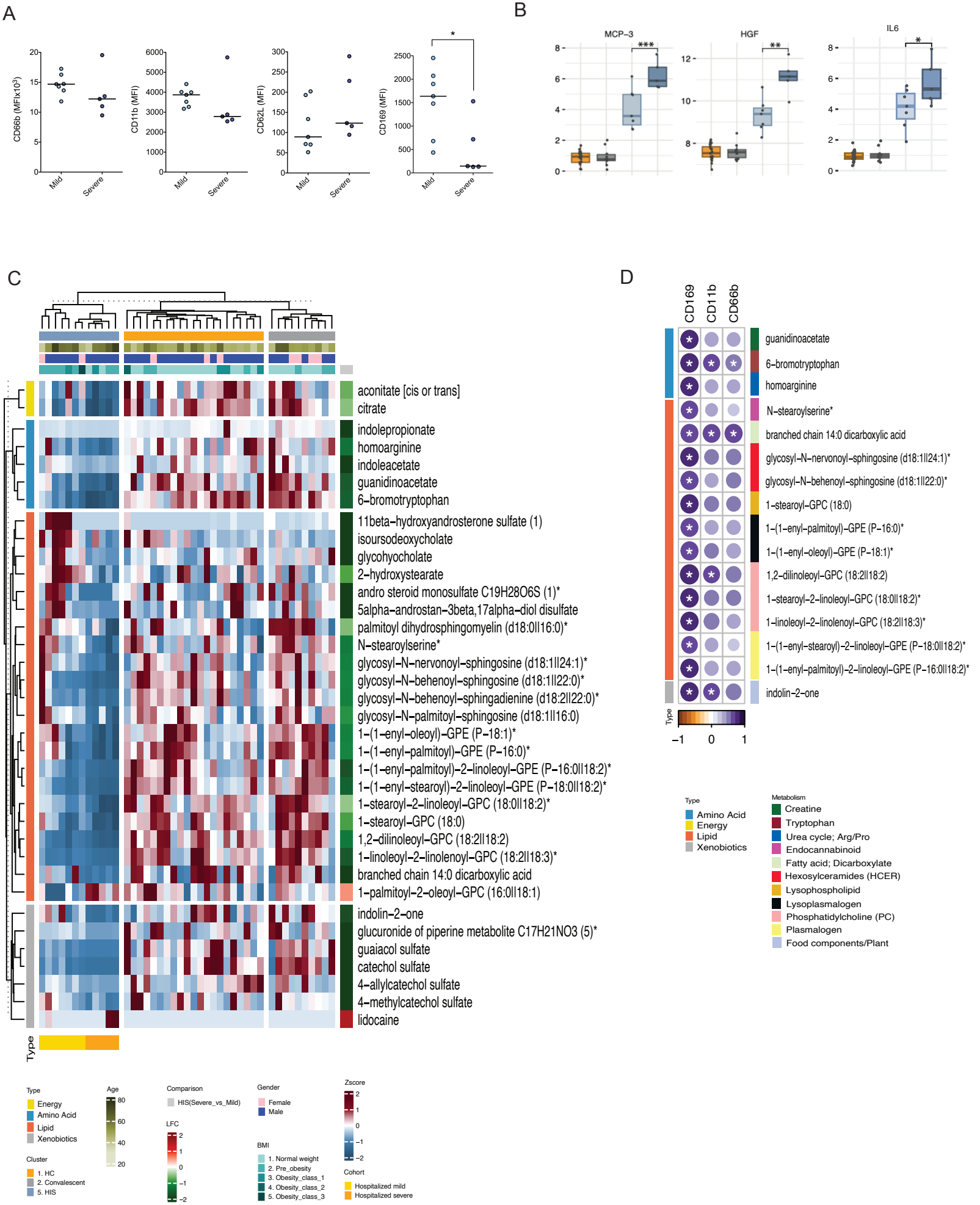
A
CD66b (MFIx10³)
CD11b (MFI)
CD62L (MFI)
CD169 (MFI)
Mild
Severe
B
MCP−3
HGF
IL6
C
aconitate [cis or trans]
citrate
indolepropionate
homoarginine
indoleacetate
guanidinoacetate
6−bromotryptophan
11beta−hydroxyandrosterone sulfate (1)
isoursodeoxycholate
glycohyocholate
2−hydroxystearate
andro steroid monosulfate C19H28O6S (1)*
5alpha−androstan−3beta,17alpha−diol disulfate
palmitoyl dihydrosphingomyelin (d18:0|l16:0)*
N−stearoylserine*
glycosyl−N−nervonoyl−sphingosine (d18:1|l24:1)*
glycosyl−N−behenoyl−sphingosine (d18:1|l22:0)*
glycosyl−N−behenoyl−sphingadienine (d18:2|l22:0)*
glycosyl−N−palmitoyl−sphingosine (d18:1|l16:0)
1−(1−enyl−oleoyl)−GPE (P−18:1)*
1−(1−enyl−palmitoyl)−GPE (P−16:0)*
1−(1−enyl−palmitoyl)−2−linoleoyl−GPE (P−16:0|l18:2)*
1−(1−enyl−stearoyl)−2−linoleoyl−GPE (P−18:0|l18:2)*
1−stearoyl−2−linoleoyl−GPC (18:0|l18:2)*
1−stearoyl−GPC (18:0)
1,2−dilinoleoyl−GPC (18:2|l18:2)
1−linoleoyl−2−linolenoyl−GPC (18:2|l18:3)*
branched chain 14:0 dicarboxylic acid
1−palmitoyl−2−oleoyl−GPC (16:0|l18:1)
indolin−2−one
glucuronide of piperine metabolite C17H21NO3 (5)*
guaiacol sulfate
catechol sulfate
4−allylcatechol sulfate
4−methylcatechol sulfate
lidocaine
Type
Type
Energy
Amino Acid
Lipid
Xenobiotics
Cluster
1. HC
2. Convalescent
5. HIS
Age
Comparison
HIS(Severe_vs_Mild)
LFC
Gender
Female
Male
BMI
1. Normal weight
2. Pre_obesity
3. Obesity_class_1
4. Obesity_class_2
5. Obesity_class_3
Zscore
Cohort
Hospitalized mild
Hospitalized severe
D
CD169
CD11b
CD66b
guanidinoacetate
6−bromotryptophan
homoarginine
N−stearoylserine*
branched chain 14:0 dicarboxylic acid
glycosyl−N−nervonoyl−sphingosine (d18:1|l24:1)*
glycosyl−N−behenoyl−sphingosine (d18:1|l22:0)*
1−stearoyl−GPC (18:0)
1−(1−enyl−palmitoyl)−GPE (P−16:0)*
1−(1−enyl−oleoyl)−GPE (P−18:1)*
1,2−dilinoleoyl−GPC (18:2|l18:2)
1−stearoyl−2−linoleoyl−GPC (18:0|l18:2)*
1−linoleoyl−2−linolenoyl−GPC (18:2|l18:3)*
1−(1−enyl−stearoyl)−2−linoleoyl−GPE (P−18:0|l18:2)*
1−(1−enyl−palmitoyl)−2−linoleoyl−GPE (P−16:0|l18:2)*
indolin−2−one
Type
Type
Amino Acid
Energy
Lipid
Xenobiotics
Metabolism
Creatine
Tryptophan
Urea cycle; Arg/Pro
Endocannabinoid
Fatty acid; Dicarboxylate
Hexosylceramides (HCER)
Lysophospholipid
Lysoplasmalogen
Phosphatidylcholine (PC)
Plasmalogen
Food components/Plant